

Generalised parametric functions and spatial correlations for seismic velocities in the Canterbury, New Zealand region from surface-wave-based site characterisation



Ethan M. Thomson^a, Brendon A. Bradley^a, Robin L. Lee^{a,*}, Liam M. Wotherspoon^b, Clinton M. Wood^c, Brady R. Cox^d

^a Department of Civil and Natural Resources Engineering, University of Canterbury, Christchurch, New Zealand

^b Department of Civil and Environmental Engineering, The University of Auckland, Auckland, New Zealand

^c Department of Civil Engineering, University of Arkansas, Fayetteville, AR, 72701, United States

^d Department of Civil, Architectural and Environmental Engineering, The University of Texas, Austin, TX, 78712, United States

ARTICLE INFO

Keywords:

Shear-wave velocity
Spatial correlations
Velocity perturbations
Canterbury sedimentary basin
New Zealand

ABSTRACT

This paper presents the development of depth- and V_{30} -dependent parametric velocity and spatial correlation models to characterise shear-wave velocities within the geologic layers of the Canterbury New Zealand sedimentary basin. The models utilise data from 22 shear-wave velocity profiles of up to 2.5km depth, derived from surface wave analysis, juxtaposed with models which detail the three-dimensional structure of the geologic formations in the Canterbury sedimentary basin. Parametric velocity equations are presented for Fine Grained Sediments, Gravels, and Tertiary layer groupings. Spatial correlations were developed and applied to generate three-dimensional stochastic velocity perturbations. Dispersion curves for the stochastic models and observed velocity profiles show good agreement over a wide frequency range with the dispersion data underlying the velocity profiles used as input data, indicating that the parametric perturbed velocity profiles replicate the dispersion characteristics of the observed velocity profiles. Collectively, these models enable seismic velocities to be realistically represented for applications such as 3D ground motion and site response simulations.

1. Introduction

The 2010-2011 Canterbury, New Zealand, earthquake sequence produced strong ground motions in Canterbury and urban Christchurch causing significant damage to structural and geotechnical systems [1,2]. The complex three-dimensional geologic structure of the Canterbury sedimentary basin was a likely salient factor in the appreciable spatial variability of ground motions, as the soft sedimentary deposits resulted in both basin and nonlinear near-surface soil response effects that have been investigated empirically [3,4] and through physics-based ground motion simulations [5,6]. Ongoing examination of these factors via 3D physics-based ground motion and site response simulations require detailed models of the three-dimensional geologic and velocity structure of the Canterbury sedimentary basin.

The regional geology in Canterbury consists of Interbedded Quaternary Gravels and Fine Grained Sediments in urban Christchurch [7,8] which overlie Tertiary deposits and subsequent geologic basement

[9,10]. Geologic surface models that define the three-dimensional structure of different geologic units have been developed for the Canterbury sedimentary basin [11,12]. The structure of the near surface, $z < 500m$, Quaternary deposits (gravels interbedded with silts, clays, peat, and shelly sands) was mapped by Lee et al. [11], and the deep structure, $z > 500m$, of Neogene (Late Tertiary) and Paleogene (Early Tertiary) deposits have been detailed by Lee et al. [12]. Seismic velocities within the different geologic units in Canterbury have been investigated by a number of researchers. Velocities for the Tertiary deposits have been investigated by Lee et al. [12] based on correlations with P-wave (V_p) travel times from seismic reflection lines and well logs in combination with migration and interval velocities from Barnes et al. [13] to specify constant V_p velocities for each of the Tertiary units. Given the inability to develop more complex and realistic models without robust data, shear-wave (V_s) estimates were subsequently derived from the empirical relationships of Brocher [14]. The adoption of constant velocities for a given geologic unit fails to accurately

* Corresponding author.

E-mail addresses: ethan.thomson@pg.canterbury.ac.nz (E.M. Thomson), brendon.bradley@canterbury.ac.nz (B.A. Bradley), robin.lee@canterbury.ac.nz (R.L. Lee), l.wotherspoon@auckland.ac.nz (L.M. Wotherspoon), cmwood@uark.edu (C.M. Wood), brcox@utexas.edu (B.R. Cox).

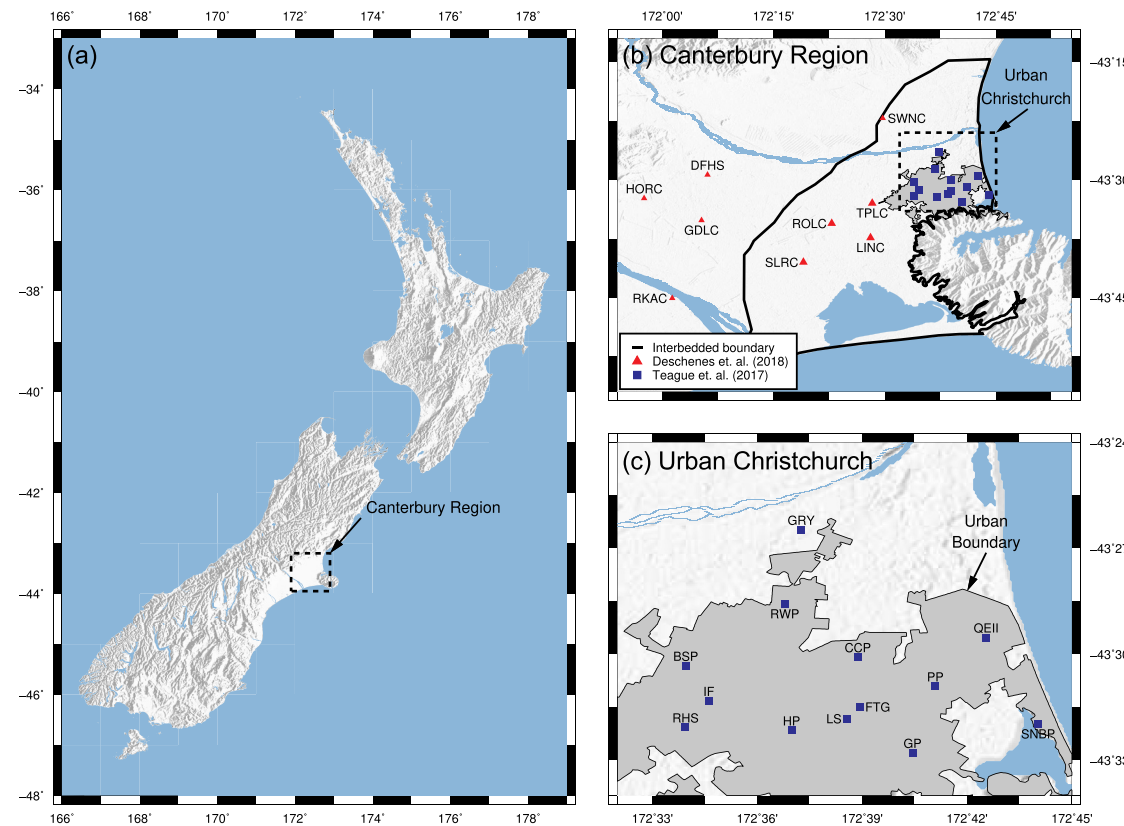


Fig. 1. (a) Location of the Canterbury region within New Zealand; (b) spatial distribution of the 22 velocity profiles used in this study in the Canterbury region, and (c) urban Christchurch.

characterise velocity variations (with depth principally, but also laterally) and results in artificially large velocity contrasts at geologic boundaries. This simplified velocity prescription is also problematic when a geologic unit outcrops as the velocities can be unrealistically high. Additionally, prescription of constant velocities is too simplistic for simulating high frequencies.

Two recent studies [15,16] have developed deep V_s velocity profiles as a function of depth (z) using surface-wave-based methods, which offer the potential to develop more detailed representation of velocity structure across the entire Canterbury sedimentary basin. Teague et al. [15] proposed a depth-dependent parametric V_s equation to prescribe shear wave velocities within the Riccarton Gravels (the shallowest gravel layer in urban Christchurch) and noted the large regional velocity variability. Deschenes et al. [16] proposed three unique depth-dependent parametric equations to characterise shear-wave velocities in the Quaternary units. These equations prescribe velocities to three groups of Quaternary deposits: Interbedded Gravels, Non-Interbedded Gravels and Fine Grained Sediments (i.e. sands and silts). Deschenes et al. [16] utilised two separate equations to prescribe Gravel velocities, which can lead to an unintended discontinuity at the lateral Interbedded - Non-Interbedded boundary, which would not exist with a single unified equation.

Modelling velocity heterogeneities is important for physics-based wave propagation models as they contribute to scatter which excites coda waves [17,18] that have implications in ground motion modelling [19–21]. Given a paucity of data it is not presently possible to deterministically represent velocity heterogeneities at fine spatial scales. However, a simplistic statistical model that replicates velocity variability from observations can be used as a means of representing small-scale velocity heterogeneities. Such models utilise spatial correlations developed from geostatistical analysis to generate velocity perturbations.

This paper presents the development of parametric velocity functions that prescribe shear wave velocity as a function of depth and V_{s30} , based on 22 observed velocity profiles distributed throughout urban

Christchurch and the Canterbury region [15,16]. The developed parametric functions prescribe velocities to the 11 geologic units of the Canterbury sedimentary basin grouped into three distinct geologic categories: Fine Grained Sediments, Gravels and Tertiary deposits. Spatial correlations are developed that can be applied to generate velocity perturbations that replicate the velocity variability within the observed velocity profiles. Together the parametric velocity functions with spatial correlations and regional geologic surface models are applied to generate one-dimensional velocity profiles, two-dimensional velocity transects and three-dimensional velocity models of the Canterbury sedimentary basin, all with small-scale stochastic heterogeneities. Finally, as one means of independently demonstrating validity, dispersion curves for the stochastic models are then compared with the dispersion data underlying the surface-wave derived velocity profiles.

2. Data sources

The adopted datasets for developing the parametric functions and spatial correlations comprise shear-wave velocity profiles and stratigraphic profiles of the geologic structure. The velocity profiles are distributed throughout Canterbury and detail the one-dimensional velocity structure at a site, while stratigraphic profiles are derived from geologic surface models which detail the regional geologic structure. The following subsections present details of these two datasets. It is acknowledged that both of these datasets represent model-derived data as opposed to direct measurements, but for brevity herein we simply refer to them as 'data'.

2.1. Shear wave velocity profile data

Shear wave velocity profiles from two studies at sites located throughout urban Christchurch [15] and the wider Canterbury region [16] are utilised. Due to the complexities involved with generating velocity profiles (requirements for specialist equipment and knowledge,

intricacies associated with data acquisition and processing) these were the first studies to generate deep velocity profiles in Canterbury. Note that for the purposes of this work, deep ($z > 500\text{m}$) profiles were desired, and therefore we ignore other ‘shallow’ investigations in the region [e.g. [22]].

Fig. 1 presents the location of the Canterbury region within New Zealand and the spatial distribution of shear wave profiles from the two studies. Both Teague et al. [15] and Deschenes et al. [16] utilised surface wave analysis methods to characterise the velocity structure at a site. Active source Multi-channel Analysis of Surface Waves (MASW) [23] and passive source Microtremor Array Method (MAM) [24] techniques were employed to generate dispersion curves for each site, which were then inverted using apriori subsurface information (e.g. depths to geologic horizons, discussed further in Section 2.2) to yield a site-specific velocity profile. As this inversion is non-unique, a number of velocity profiles were generated for each site which fit the observed dispersion data equally well. Specifically, both Teague et al. [15] and Deschenes et al. [16] present 1000 lowest misfit profiles, and the median of these profiles was utilised in this study. As an illustration, **Fig. 2** presents median profiles from two sites in Canterbury. The characteristics of the velocity profiles are dependent on their region of origin. Specifically, profiles can exhibit reversals if they are located within the interbedded region (see **Fig. 1**) while sites outside of this region do not. Profiles are prescribed as layered earth models comprised of multiple layers, between which constant shear wave velocities are applied.

The maximum depth of the velocity profiles varies from approximately 500 – 2500m, with profiles terminating at the geologic basement or the Banks Peninsula Volcanics, signified by a significant increase in velocity. In total, 22 median velocity profiles were utilised in this study with 13 located within Christchurch [15] and 9 within the wider Canterbury region [16].

2.2. Regional geology models

The geologic structure of the Canterbury sedimentary basin has been recently modelled by Lee et al. [11] and Lee et al. [12], drawing on prior work of Brown et al. [8], Talbot et al. [25], White and Della Pasqua [26] for Quaternary units and Forsyth et al. [9], Hicks [10],

Ghisetti and Sibson [27] for Tertiary units. Lee et al. [11,12] collectively detail the three-dimensional geologic structure of eight Christchurch Interbedded and three Canterbury Tertiary deposits respectively, which were developed using a combination of cone penetration tests, well logs, seismic reflection lines and regional geologic maps spanning multiple length scales.

Lithological differences exist throughout the region due to marine regressions and transgressions, resulting in interbedded gravels and fine-grained sediments in urban Christchurch [7]. **Fig. 3** presents an East-West cross section through the interbedded layers within Christchurch. This interbedded structure ceases inland where the fine-grained sediment formations taper to zero thickness, the boundary of this interbedded region corresponds to historic sea levels and can be seen in **Fig. 1**. Below these layers lie Tertiary deposits and subsequently geologic basement.

2.3. Attribution of data to geologic layers

Velocity profiles at the 22 sites in **Fig. 1** were developed utilising geologic layer depths from Lee et al. [11] and Lee et al. [12] as constraints which were allowed to vary within pre-defined vertical uncertainty bounds. Therefore, the exact depths of the geologic surfaces (interpolated from the Lee et al. [11,12] geologic surface models) differ in the predictive model from those of the profiles generated from inversion. However, as this difference is relatively small, the profiles can be decomposed and the constituent sections attributed to one of the 11 distinct geologic formations.

The velocity profiles are layered models that assume constant velocities within each layer, as a simplification of a more continuous variation with depth. As a result, the centre depth and velocity of each layer are adopted to represent the respective layer as discrete points for subsequent analysis. The number of layers used to model velocities within different geologic formations in a velocity profile varies with the thickness of the formation, with some deposits modelled by two or more layers. These points enable profile sections corresponding to specific geologic formations to be grouped and analysed together. As an example, **Fig. 4** illustrates how the profile at LINC was analysed using the geologic surface depths at this location to attribute velocities to geologic formations (note that the depth from geologic surface models are not an exact match with the velocity profiles due to the inversion

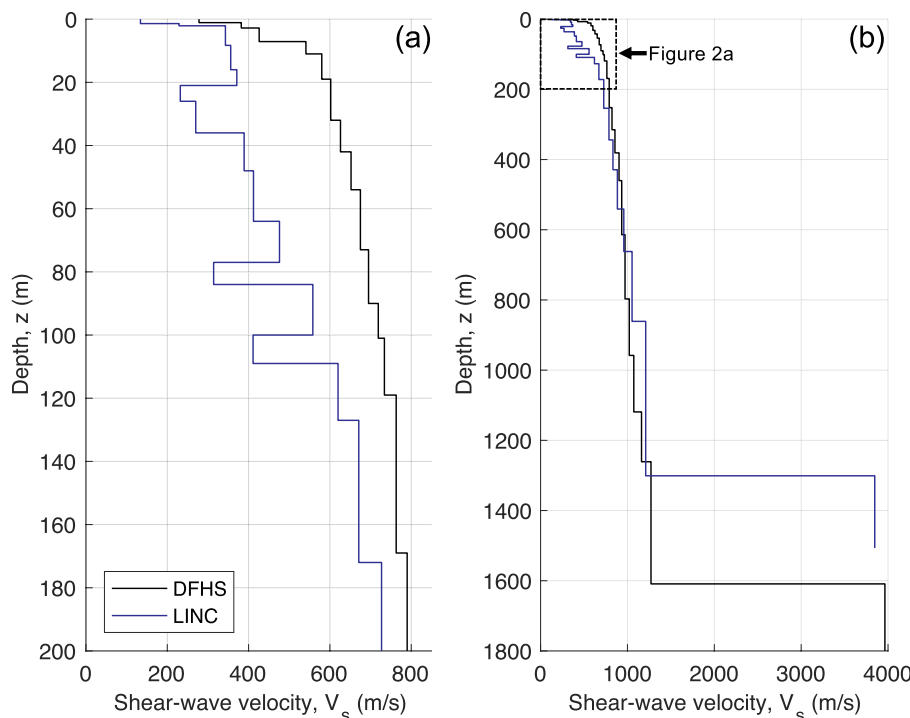


Fig. 2. Examples of shear-wave velocity profiles from strong motion sites DFHS and LINC with two depth scales for examining shallow and deep velocities. The velocity structure at LINC exhibits velocity reversals as a result of interbedded gravel and fine grained-sediment layers, while the gravel-dominated quaternary deposits at DFHS site exhibit monotonically increasing velocities (see **Fig. 1**).

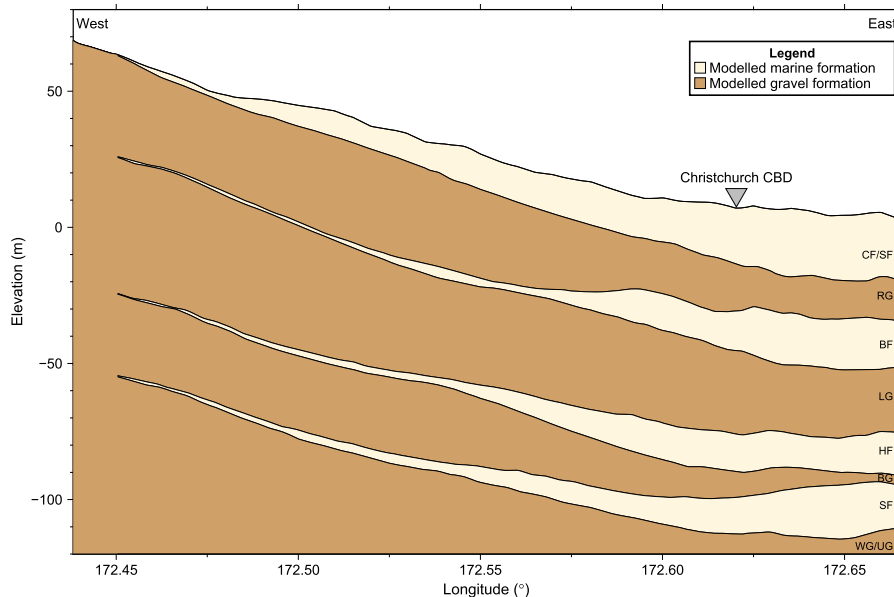


Fig. 3. Schematic East-West cross-section of the interbedded geologic structure in Canterbury with marine formations (deposited during marine transgressions when sea levels are high) tapering to zero thickness in the westward direction. Formation acronyms in the right of the figure are presented in Table 1 [After 11, 16].

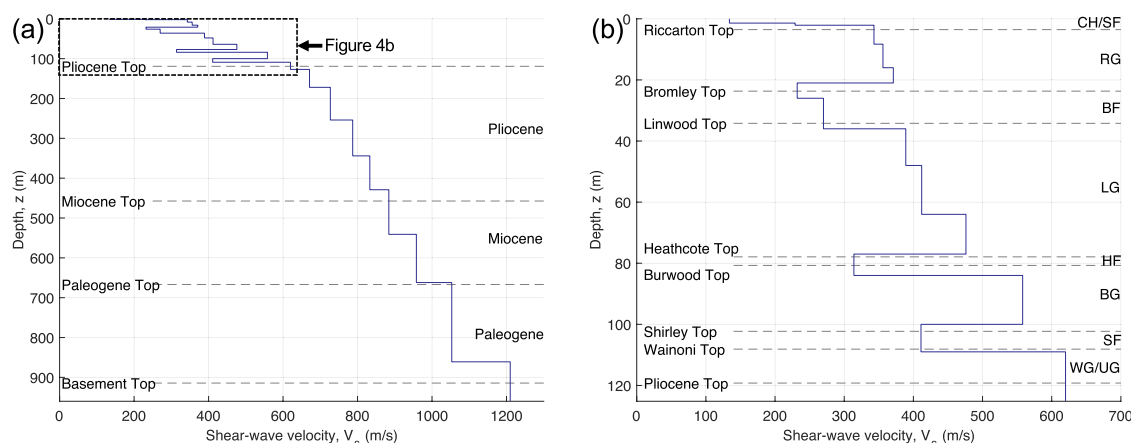


Fig. 4. Median V_s profile at site LINC illustrating attribution to different geologic formations.

process allowing these to vary). Not all layers from the original profiles were used as some represented unrealistic velocities, these typically occurred in the Banks Peninsula Volcanics or at large depths within the assumed geologic basement.

Developing unique parametric functions for each of the 11 distinct Canterbury layers (Fig. 3) was not possible due to data paucity. As a result, layers were grouped into three geologic categories for this analysis as noted in Table 1: Fine Grained Sediments, Gravels and Tertiary deposits. Fine Grained Sediments and Gravels, deposited during cyclic marine transgressions and regressions [7,11], differ significantly in composition with Gravels being stiffer with higher velocities, for a given confining pressure, than Fine Grained Sediments. Below these Interbedded layers are three Tertiary deposits of variable composition overlying the geologic basement [12].

3. Parametric velocity equation development

3.1. Model formulation

Previous research has utilised polynomial- and exponential-type models to characterise geologic shear wave velocity as a function of depth. Polynomial functions were used, for example, in the United

Table 1

Geologic unit groupings used in the construction of parametric velocity functions.

Layer Grouping	Geologic layers
Fine Grained Sediments	Christchurch/Springston (CF/SF) Bromley (BF) Heathcote (HF) Shirley (SF)
Gravels	Riccarton (RG) Linwood (LG) Burwood (BG) Wainoni/Undifferentiated (WG/UG)
Tertiary	Pliocene Miocene Paleogene

States Geological Survey velocity model of the San Francisco Bay Area [28] which employed numerous distinct polynomial equations to characterise velocities in different geologic units. A Central Eastern United States velocity model [29] utilises a polynomial function to characterise the near surface velocity structure.

Exponential models have been utilised, for example, in a velocity model of Southern California [30] which employed the exponential model of Faust [31]. Deschenes et al. [16] presents models for the Canterbury region based on the exponential form of Lin et al. [32] for application to three different geologic settings in Canterbury with an additional median representative fit for the region. With sufficient empirical data for constraint there are no conceptual differences between the use of polynomial or exponential functions, however some polynomial functional forms can be non-physical when extrapolated, and thus typically require depth constraints in their application [e.g. 29].

Depth is a general parameter utilised in all velocity prescribing equations, as a substitute for confining pressure, with some functions additionally supplementing this with age [31] and V_{s30} (the time-averaged shear-wave velocity in the top 30 m) [29]. Age was considered an unnecessary term for inclusion within the parametric velocity functions in this study, as it is essentially a proxy for depth when sediments are sequentially deposited and significant uplift has not occurred over the period of interest, as is the case in the Canterbury sedimentary basin. A V_{s30} dependence allows near surface velocity information to be incorporated within estimates for deeper ($z > 30m$) velocities and therefore was adopted for inclusion as discussed subsequently.

Three exponential-type functional forms were considered in this study, each of which adds an additional parameter to characterise velocities: the first parametrisation is an exclusively depth-dependent functional form, Equation (1); the second incorporates a V_{s30} term within the prediction, Equation (2); and the third implements a V_{s30} taper to restrict the effect of V_{s30} to only influence the velocities in the near surface, Equation (3).

The mathematical formulation for the depth-dependent functional form is

$$\ln(V_s) = \ln(a) + b\ln(z) \quad (1)$$

where z is the depth, a and b are constants, and \ln is the natural logarithm. Building on this formulation, the second functional form, which incorporates V_{s30} , is

$$\ln(V_s) = \ln(a) + b\ln(z) + \ln(c) + d\ln(V_{s30}) \quad (2)$$

where c and d are constants. It is possible to reduce the number of constants in Equation (2), however, due to the incremental construction technique used in Section 3.2 these constants are kept independent which allows for the same values for the constants to be applied to all three functional forms. The final functional form, building on Equation (2) by introducing a tapering of the V_{s30} term is

$$\ln(V_s) = \ln(a) + b\ln(z) + \exp[-(z/e)^f][\ln(c) + d\ln(V_{s30})] \quad (3)$$

where e and f are constants. Depth was adopted as the primary predictor as confining pressure increases with depth, which subsequently

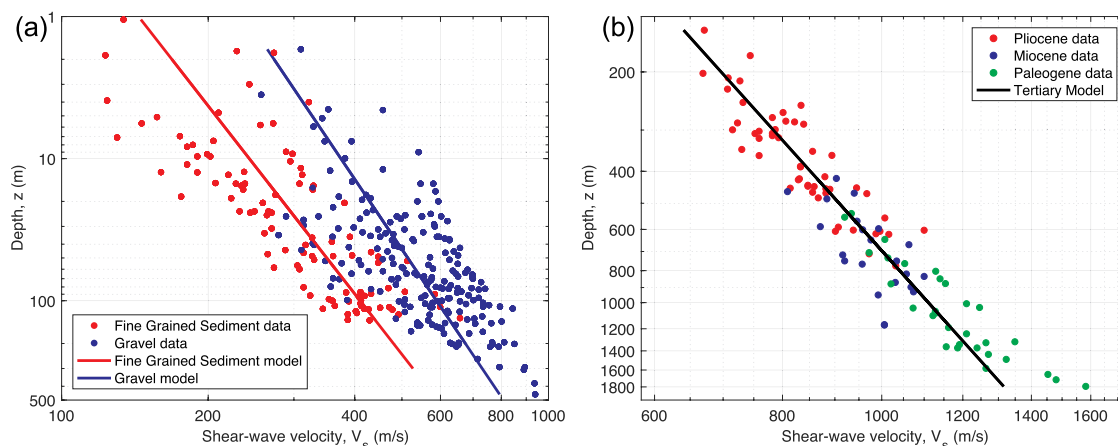


Fig. 5. Depth-dependent models for: (a) Interbedded Gravels and Fine Grained Sediments; and (b) Tertiary layer groupings.

increases velocities. The inclusion of a V_{s30} term allows for near surface velocities to aid in the prescription of deeper ($z > 30m$) velocities. The tapering of the V_{s30} term reduces its effect with depth (and therefore should not affect predictions when $z > 30m$), since V_{s30} contains physical information for only the upper 30 m of the crust. The fitting of the coefficients to these functional forms for the Canterbury data is presented in Section 3.2.

When fitting parametric functional forms to the observed velocities (Section 3.2) analysing prediction residuals allows systematic trends to be identified and models to be refined. Prediction residuals for a single velocity observation can be calculated using the classical residual formulation of

$$\ln(V_{obs}) = \ln(V_{pred}) + \Delta \quad (4)$$

where V_{obs} is the observed velocity, V_{pred} is the predicted velocity via Equations (7)–(9) and Δ is the total residual. Using mixed effects regression [33], the total residual can be apportioned into between- and within-site residuals (δb_s and δw , respectively) using

$$\Delta = \delta b_s + \delta w \quad (5)$$

δb_s represents the mean difference between the observed and modelled velocities for all observations at an individual site, while δw is the ‘remaining’ residual for a single velocity observation and represents the unexplained behaviour not captured by the model or δb_s . Both δb_s and δw are assumed as independent normally distributed with zero mean and standard deviations of $\sigma_{\delta b_s}$ and $\sigma_{\delta w}$, respectively. The total standard deviation is then defined as:

$$\sigma_{\ln V_s} = \sqrt{\sigma_{\delta b_s}^2 + \sigma_{\delta w}^2}. \quad (6)$$

3.2. Application to data

3.2.1. Depth-dependency

Depth-dependent exponential models were fitted to the three layer groupings using the functional form presented in Equation (1). Fig. 5 illustrates the exponential models for the three layer groupings. Coefficients for the three models and the depth range of the observed velocities utilised in generating these are shown in Table 2. The depths of the observed velocities, which were utilised in generating the depth-dependent fit, vary by layer grouping. The observed velocities of the Gravel layer grouping extend to greater depths than the Fine Grained Sediment layers, especially in West Canterbury outside of the Interbedded boundary, where the stratigraphy is exclusively gravels from the ground surface through to the Tertiary deposits. The depth range from the velocity profiles distributed throughout Canterbury do not represent the full range of depths we aim to be able to prescribe velocities at. Geologic

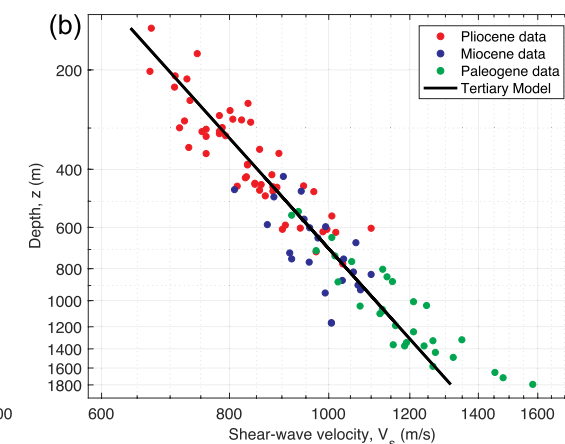


Table 2
Depth-dependent model coefficients (Equation (1)).

Layer grouping	a	b	Depth range of observed velocities (m)
Fine grained sediments	144	0.228	0-150
Gravels	238	0.197	0-500
Tertiary	150	0.290	150-1800

deposits can occur outside of the ranges of the original velocity profiles, therefore generating realistic parametric velocity equations that can be extrapolated beyond the depths of the observed velocities which they are conditioned on is important to be able to prescribe the velocities for the entire Canterbury sedimentary basin.

Fig. 6 presents the fitted depth-dependent parametric velocity functions for the Gravel and Fine Grained Sediment layers for comparison with previous depth-dependent velocity prescriptions for Christchurch proposed by Deschenes [34] and reference velocity curves from Lin et al. [32]. The two velocity curves from Deschenes [34] were developed from the Teague et al. [15] Christchurch profiles, and can be used to prescribe velocities up to 500 m, the depth at which these curves converge. At depths greater than 500 m, Deschenes [34] utilises one model to prescribe all velocities independent of geologic type. A comparison with the depth-dependent model for the Fine Grained Sediments reveals Deschenes [34] predicts higher velocities for $z > 35$ m, which may be a result of the enforced convergence of the Deschenes [34] Gravel and Sediment models at $z = 500$ m.

3.2.2. V_{s30} -Dependency

Fig. 7 presents the relationship of V_{s30} and the between-site residuals (δb_s) from the depth-dependent model (obtained here directly from the observed velocity profile) for the Gravels and Fine Grained Sediments. The dependence of δb_s on V_{s30} , shown by the positive linear trends, suggests that there is relative bias in the prediction of V_s with respect to V_{s30} . The positive trends indicate that V_s for low V_{s30} sites are systematically overpredicted relative to high V_{s30} sites. As V_{s30} is a strong predictor of the velocities in the interbedded layers at a site, this warrants its inclusion in the prediction functional form. Analysing the

between-site residual for the Tertiary layers indicated that V_{s30} did not have a strong relationship with δb_s (as would be expected given the depth of Tertiary deposits).

Table 3 presents the coefficients for the depth- and V_{s30} -dependent parametric function (Equation (2)) for the Gravel and Fine Grained Sediment layer groupings. Mathematically, the coefficients a and c could be combined to form a new constant (see Equation (2)), however, they are presented here separately such that the same values for the coefficients are applicable in Equations (1)–(3).

3.2.3. Tapering of V_{s30} -dependence with depth

The V_{s30} -dependency developed in Section 3.2.2, and given by Equation (2), is constant with depth. However, its physical importance should diminish with increasing depth because V_{s30} should not be predictive of velocities at depth $z > 30$ m. Further modification is therefore necessary to ensure that the influence of V_{s30} appropriately diminishes with depth. Equation (3) introduces an exponential decay term for tapering of the V_{s30} effect, where the parameters e and f are defined to scale the spatial length and rate of transition over which the taper is applied. Larger values of e are associated with the tapering being applied over a larger depth range, while increasing the f coefficient increases the rate at which the effect of the taper reduces to zero. There were two primary considerations in the adoption of these coefficients; first the length over which the taper is applied should seek to minimise the misfit with observed data; and second is minimising the amount of unintended velocity reversals that could occur at the modelled Gravel - Tertiary layer interface - these reversals typically occur as this interface tends toward the ground surface ($z < 50$ m), where the Tertiary equation for velocity is unconstrained by observed data (i.e. Fig. 5b for $V_s < 600$ m/s). Velocity reversals are not always non-physical, for example, the transition from Gravels to Fine Grained Sediments often has a reversal (e.g. Fig. 2). Undesirable velocity reversals are those that occur away from geologic boundaries where we expect this behaviour. E.g. we expect velocity reversals at specific geologic transitions due to the relative composition of different layers, the velocity reversal at the transition from stiff gravels to fine-grained-sediments is expected, while the velocity reversal at the transition from the gravel to the tertiary layer at 120 m in Fig. 12 is not desired as we expect velocities

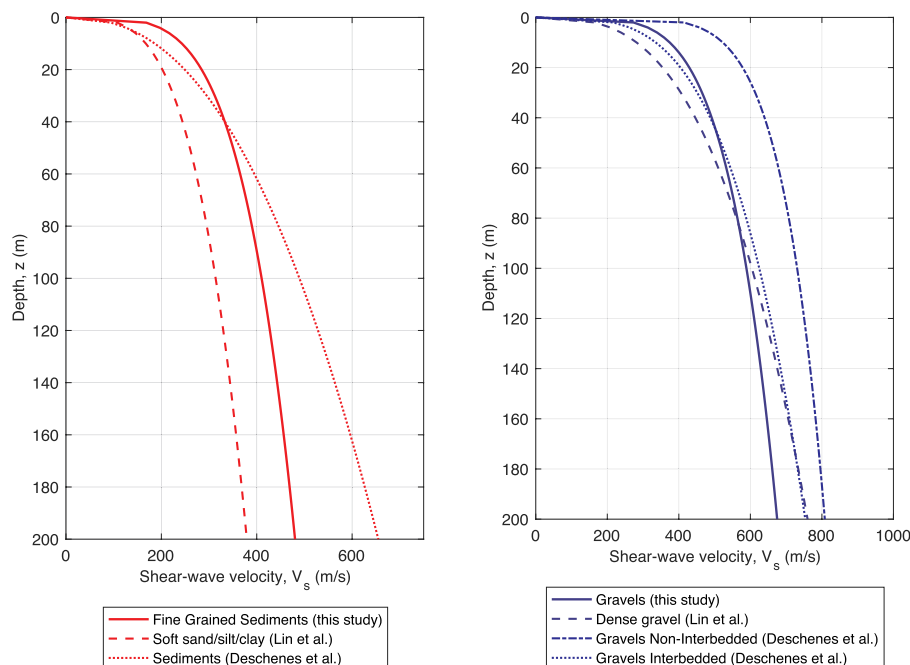


Fig. 6. Comparison of depth-dependent models for Fine Grained Sediments and Gravel layer groupings from this study with reference models [32] and previous Canterbury specific velocities [16].

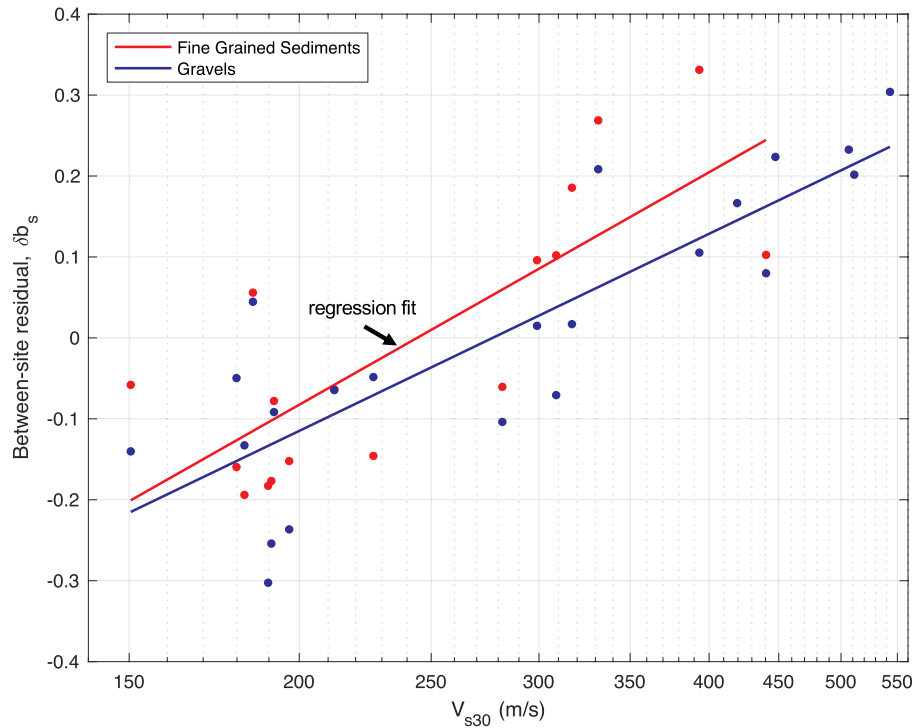


Fig. 7. Correlation between V_{s30} and grouping-specific between-site residual, δb_s .

Table 3
Depth- and V_{s30} -dependent model coefficients (Equation (2)).

Layer grouping	a	b	c	d
Fine Grained Sediments	144	0.228	0.0966	0.425
Gravels	238	0.197	0.138	0.351

to only increase at this geologic boundary.

A minimum velocity for the Tertiary layers can be enforced to reduce non-physical velocity reversals at the Gravel-Tertiary interface, and to prevent excessive extrapolation beyond the depths of velocity observations. Therefore $V_{s,min} = 600\text{m/s}$ was implemented for the Tertiary layers to reduce undesirable velocity reversals, this value is based on the lowest observed velocity for the Tertiary layers.

Using a regional V_{s30} model [35] in combination with the geologic surface model for the Gravel-Tertiary interface [12], a parametric analysis was conducted to determine the optimal values for e and f considering the number of non-physical velocity reversals in Canterbury and the total misfit (i.e. the sum of the absolute value of the total residual for all observed velocities). This lead to $e = 40$ and $f = 2$ being adopted as the tapering coefficients for both the Gravel and Fine Grained Sediment models. Fig. 8 illustrates the velocity ratio contrast at the Gravel-Tertiary interface across Canterbury. It can be seen that some regions (approximately 5.6% of the total area) exhibit velocity reversals for the adopted tapering coefficients, however, the magnitude of these reversals are insignificant (<2.5%).

Fig. 9 presents how the adopted V_{s30} tapering affects the Gravel and Fine Grained Sediment velocities in the near surface region for different V_{s30} values.

3.3. Adopted models

The depth-dependent parametric function was adopted to prescribe velocities in the Tertiary layers, because it was deemed that a V_{s30} -dependence was not justified. Additionally a minimum velocity was enforced for the Tertiary layers. The adopted function to prescribe

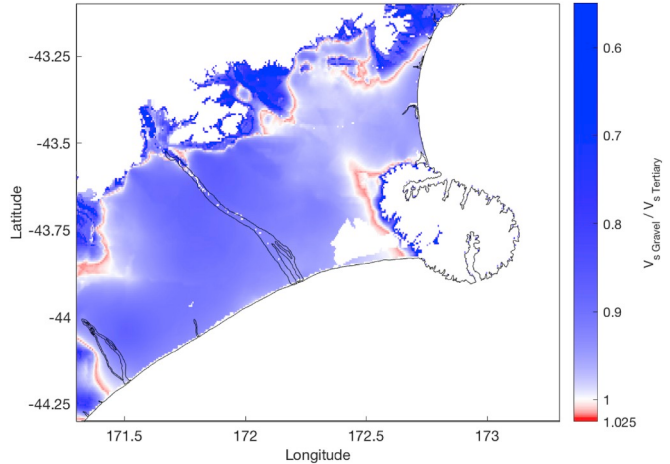


Fig. 8. Velocity ratio at the Gravel-Tertiary interface in Canterbury. Values <1 indicate a velocity increase from the Gravel to the Tertiary layer while values >1 indicate a decrease in velocity from Gravel to Tertiary deposits (i.e. velocity reversal).

velocities to the Tertiary layers is

$$\ln(V_s) = \begin{cases} \ln 600 & \text{for } z \leq 119\text{m} \\ \ln 150 + 0.290 \ln(z) & \text{for } z > 119\text{m} \end{cases} \quad (7)$$

where z is the depth in meters and 600m/s represents the minimum shear-wave velocity prescribed to the Tertiary layers.

The depth with tapered V_{s30} -dependency functional form Equation (3) was adopted for the Fine Grained Sediment and Gravel layer groupings as these velocities in these layers were found to be correlated with V_{s30} . The adopted parametric models for the Fine Grained Sediment and Gravel layer groupings are

$$\ln(V_s) = 4.97 + 0.228 \ln(z) + \exp[-(z/40)^2][0.425 \ln(V_{s30}) - 2.33] \quad (8)$$

and

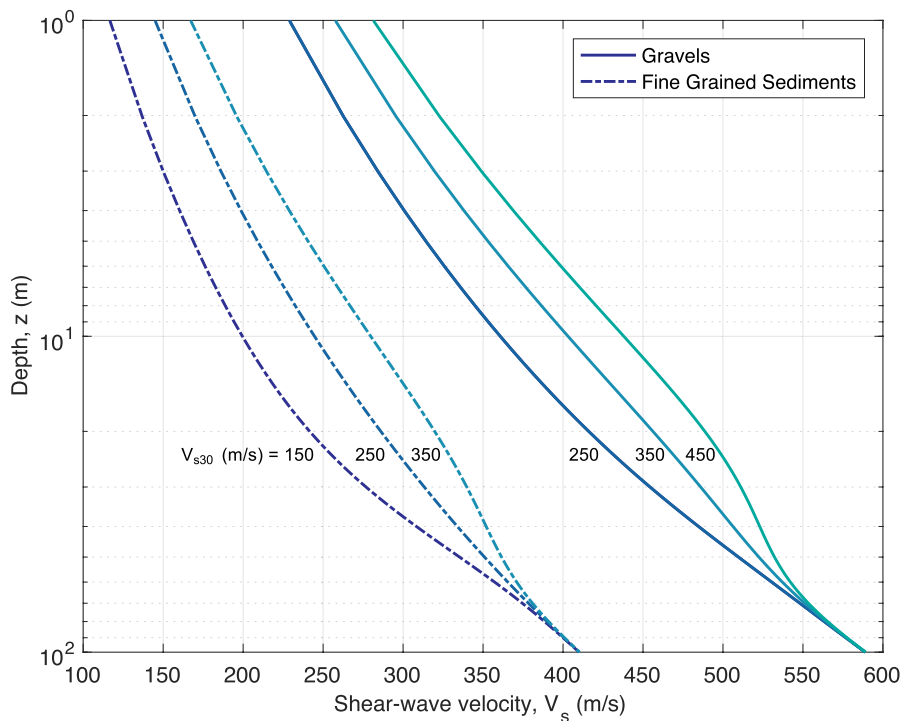


Fig. 9. Effect of V_{30} tapering for the Gravels and Fine Grained Sediments for different V_{30} conditions.

$$\ln(V_s) = 5.47 + 0.197\ln(z) + \exp[-(z/40)^2][0.351\ln(V_{30}) - 1.98] \quad (9)$$

respectively. Equations (7)–(9) provide the median prediction of $\ln(V_s)$, which has a normal distribution, and Table 4 presents the standard deviations for each of the adopted models.

4. Spatial correlations

The between- and within-site residuals (δb_s and δw , respectively) are correlated spatially, and this section examines these correlations in the horizontal and vertical planes, assuming anisotropy, using the models presented in Section 3.3. δb_s was analysed in the horizontal direction as it represents the mean difference between the parametric fit and observed velocity profile. As δw represents the unexplained velocity variation for a single velocity observation, analysing the vertical dependence of δw allows for vertical variability to be characterised and vertical correlations to be developed. Development of horizontal correlations for δw directly was not possible due to data paucity. Combining the independently-developed vertical and horizontal correlations allows for correlated velocity perturbations to be added to the parametric velocity models (discussed in Section 5.2).

4.1. Geostatistics theory

The geostatistical method of variogram analysis [36] was used to characterise the spatial variability of the residuals (details of the variogram analysis are presented in Appendix A – Variogram_analysis). Correlations are developed here by fitting theoretical variograms to empirical variograms for δb_s and δw .

Table 4
Standard deviations of adopted parametric models.

Layer grouping	$\sigma_{\ln V_s}$
Fine Grained Sediments	0.132
Gravels	0.176
Tertiary	0.062

As a summary of the results to follow, Table 5 presents parameters for fitted variograms. Empirical variograms were generated by calculating the semivariance (γ , Equation (A.1)) for pairwise observations separated by lag distance (h). Two parameters are required to fit a theoretical variogram, c and a , the sill and range, respectively (Equation (A.2) presents the functional form of the adopted exponential theoretical variogram). Adopting a realistic value for the sill is paramount when fitting a theoretical variogram. The theoretical properties of a variogram dictate that the sill is the variance of the dataset. The variance (i.e. the square of the standard deviations, Table 4) was calculated for the different geologic groupings and these values were in agreement with the sills of the theoretical fitted variograms indicating valid variogram parameters.

4.2. Between-site (horizontal) correlation

Fig. 10a illustrates empirical and theoretical variograms for δb_s . Logarithmic binning of data was utilised for the horizontal variogram to ensure a consistent number of observations within each bin. Table 5 presents the theoretical exponential variogram parameters. Trial variograms were fitted independently for δb_s to the Interbedded (Gravel and Fine Grained Sediment) and Tertiary groupings, however, a single variogram model was adopted as there was no clear distinction between the variograms from Interbedded and Tertiary groupings.

4.2.1. Spatial analysis

Analysing δb_s allows the regional horizontal velocity variability to be investigated in addition to generating horizontally correlated

Table 5
Theoretical variogram parameters for the horizontal and vertical directions.

Direction	Sill, c	Range, a
Horizontal (δb_s)	0.00918	3.89 (km)
Vertical (δw , Interbedded)	0.0210	1.02
Vertical (δw , Tertiary)	0.00758	2.15

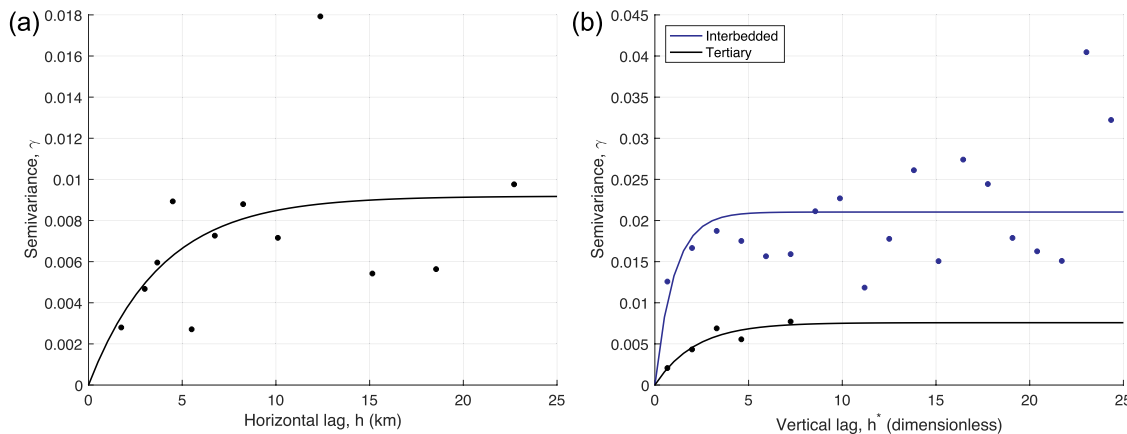


Fig. 10. Empirical and theoretical variograms: (a) between-site residual (δb_s), in the horizontal direction; and (b) within-site residual (δw) in the vertical direction.

velocity perturbations. The spatial variability of δb_s was investigated by generating a surface to illustrate its regional trend within Canterbury, which can be utilised to incorporate regional variability within the parametric velocity prescriptions. Fig. 11 presents a Kriged surface of δb_s based on the horizontal theoretical semivariogram (Fig. 10a). Within urban Christchurch δb_s is negative, indicative of the ‘baseline’ parametric models (Equation (7) to (9)) overpredicting velocities in this interbedded region, while in West Canterbury, outside of the interbedded boundary, δb_s is positive, indicating an underprediction in this region. The uncertainty associated with the Kriged surface, $\sigma_{\delta b_s}$, is zero at observation locations and increases exponentially as the distance to nearby observations increases.

4.3. Within-site (vertical) correlation

Lag distance (h) is commonly defined as the arithmetic difference between a pair of points. This definition works well in the horizontal direction, however, in the vertical direction, separation distances between observed velocities differ significantly for the Interbedded layers (0–500m) and the Tertiary layers (150–1800m). Trial variograms were independently fitted to δw for the shallow Interbedded and deep Tertiary layer, due to the differences in the depths of the observed velocities the ranges of the resulting variograms differed by an order of magnitude. Using an arithmetic definition for h it was therefore not possible to fit a single variogram that characterised all vertical layers adequately. An alternative definition for lag distance was developed Equation (10), which utilises a ratio between the depths of the pair of

points, where $z_1 \geq z_2$ and $h^* = 0$ when $z_1 = z_2$.

$$h^* = \frac{z_1}{z_2} - 1 \quad (10)$$

The benefit of such a formulation is that variability is a fractal function of depth. Fig. 10b illustrates empirical and theoretical variograms for δw . Two variograms are generated in the vertical direction, for the Interbedded and Tertiary layer groupings, respectively. The sill for the Tertiary layer groupings is lower than that of the Interbedded layers. An explanation for this is the inversion methodology utilised in the generation of the original velocity profiles. At shallow depths, the inversion is sensitive to the velocity structure, however, this sensitivity decreases with depth [23,24].

Additionally, the array geometry used to collect the surface wave data inherently limits the maximum reliable wavelength (or, lowest frequency) that can be extracted from the dispersion data. Hence, the maximum depth of reliable profiling is related to the largest array aperture used during testing. At some sites where low frequency dispersion data appeared to be coherent, Deschenes et al. [16] and Teague et al. [15] knowingly relaxed commonly assumed maximum wavelength-to-array aperture criteria in order to extend the inverted V_s profiles as deep as possible in an attempt to locate basement rock. This could be one reason why V_s for the Tertiary layers may be biased low. Additionally, it is inherently difficult to estimate bedrock/half-space velocities using surface wave methods. Lower-bound velocities for the half-space are well-constrained, but upper-bound velocities are not. Therefore, the variogram model for δw was adopted to characterise the deeper Tertiary layers.

δw varies in three-dimensions, however, due to data paucity and the relative horizontal distances between velocity observations it was not possible to constrain a horizontal variogram for δw . Therefore the range from the δb_s variogram (Table 5) was adopted to constrain the horizontal correlation of δw , allowing random realisations of δw to be simulated in up to three-dimensions (see Section 5.2). Such an assumption is made in lieu of the other de-facto assumptions of no, or perfect, horizontal correlation. Further research is required to better constrain this horizontal correlation component.

Fitted variograms can be utilised to calculate correlations. For an exponential variogram, the correlation between two points is given by

$$\rho_{i,j} = \exp\left(\frac{-h_{i,j}}{a}\right) \quad (11)$$

where $\rho_{i,j}$ is the correlation between points i and j , and $h_{i,j}$ is the lag distance. A comparison of the correlations from variogram models for δw using the ratio definition for lag (h^* , Equation (10)) and the arithmetic definition was conducted. It was found that the correlations agree over a range of depths and therefore, the ratio formulation for lag

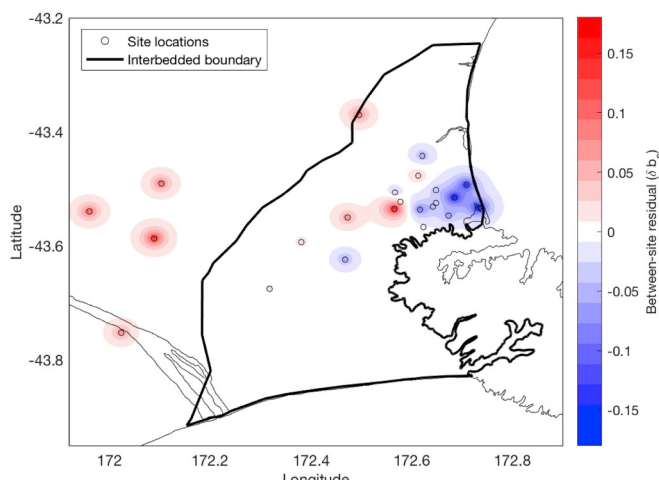


Fig. 11. Spatially-interpolated Kriged surface for the mean estimate of δb_s .

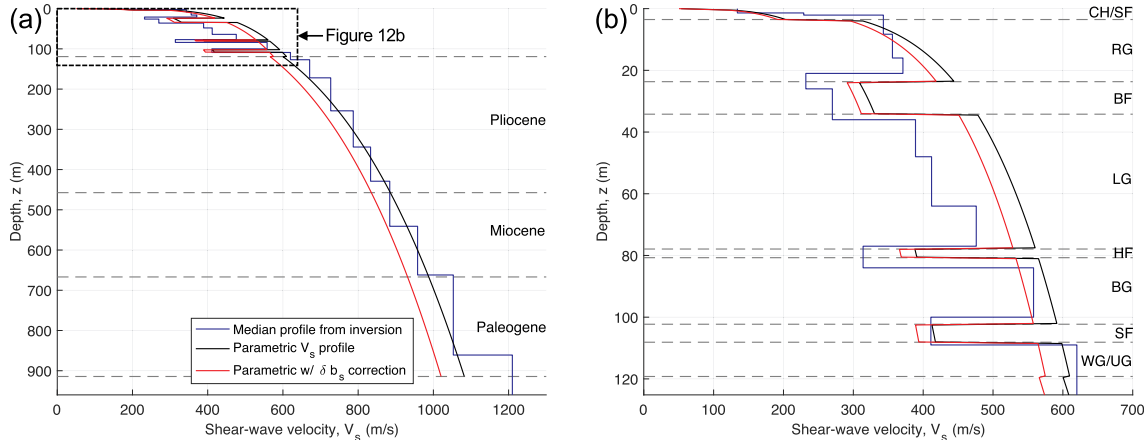


Fig. 12. Comparison of parametric velocity profile with the original profile from inversion for site LINC showing: (a) velocity profile to the geologic basement and (b). Dashed lines delineate between geologic units. (Velocity profiles for all 22 sites can be found [Appendix C](#) Vertical correlations).

distance achieves its goal of unifying all layers under one variogram model, while maintaining spatial correlations that are consistent with the arithmetic lag formulation (a figure illustrating the correlations from different variogram models is presented in [Appendix B – Vertical Correlation](#)).

5. Stochastic velocity model generation and validation

This section details the applications of the parametric functions to prescribe velocities and generation of correlated velocity perturbations which are validated via comparisons with dispersion characteristics of observed velocity profiles.

5.1. Parametric velocity profiles

Based on Equations (4) and (5), and noting that by definition the zero mean of δw and (zero) variance of $\ln(V_{pred})$, at all locations (lat, lon) the mean of the parametric model is

$$\mu_{\ln V_s}(lat, lon, z) = \ln V_{s, \text{parametric}}(lat, lon, z) + E[\delta b_s(lat, lon)] \quad (12)$$

where $\mu_{\ln V_s}$ is the mean velocity estimate, $\ln V_{s, \text{parametric}}$ is the velocity estimate from the appropriate parametric function (i.e. Equations (7)–(9)) and $E[\delta b_s]$ is the expected value of δb_s (e.g. as depicted graphically in [Fig. 11](#)). The variance of the velocity estimate can be derived from Equation (6).

[Equation \(12\)](#) is applicable in prescribing mean velocities in one-, two- or three-dimensions throughout the Canterbury sedimentary basin. The appropriate velocity parameterisation (Equation (7) to (9)) is selected by interpolating the geologic surface models for the Canterbury deposits of Lee et al. [11] and Lee et al. [12] to determine the geologic category (Gravel, Fine Grained Sediments or Tertiary) in which the point (in 3D space) is located. If the parametrisation requires a V_{s30} and no direct observation exists, a regional V_{s30} model, can be used [e.g. 35].

5.1.1. Illustrative mean parametric 1D profiles

As an example, [Fig. 12](#) presents the parametric velocity profile at site LINC (velocity profiles for all 22 sites can be found [Appendix C](#) Vertical correlations). The original median profile from inversion [16] is presented in addition to the parametric velocity profile without $E[\delta b_s]$ (see [Equation \(12\)](#)). It can be seen that the addition of the $E[\delta b_s]$ term has the general effect of improving the prediction in the near surface ($z < 120m$) Interbedded layers, while the prediction within the deep ($z > 120m$) Tertiary layers worsens. This arises from the least squares regime utilised in developing the parametric velocity functions, which decreases the overall misfit at the expense of individual velocity variations with depth.

Undesirable velocity reversals occur at the transition between the Gravel-Tertiary interface at $z = 120m$ (previously discussed in Section 3.2.3) for the site LINC as shown in [Fig. 12](#), and a number of other sites exhibit a similar behaviour. No physical evidence exists to support this reversal, although as previously noted, the magnitude of this reversal is small (<2.5% for all profiles) relative to the other uncertainties associated with velocity modelling.

5.2. Correlated velocity perturbations

Modelling of crustal heterogeneity is important for ground motion and site response simulations [37]. Scattering due to small-scale heterogeneities can have a significant effect on seismic waveforms as they generate coda waves [18]. Frankel and Clayton [38] determined the importance of modelling heterogeneities in ground motion simulation while Thompson et al. [39] investigated the effect of heterogeneities on site response.

δb_s and δw are random variables, with zero mean, which have values for observations. However, in lieu of observations, random values can be simulated and incorporated within the parametric velocity predictions to yield correlated velocity perturbations. For the case of three-dimensional random field simulations: δb_s is simulated in two-dimensions in the latitude-longitude plane to incorporate regional variability; and δw is simulated in three-dimensions to incorporate unexplained velocity variations. The dimension of the field being generated can be reduced to a two-dimensional cross section or a one-dimensional profile which reduces the dimensions that δb_s and δw are simulated in correspondingly.

Random realisations of δb_s and δw can be incorporated into velocity realisations via Equations (4) and (5):

$$\ln V_{\text{perturbed}} = \mu_{\ln V_s} + \delta b_s^* + \delta w \quad (13)$$

where $\ln V_{\text{perturbed}}$ is the natural log of the perturbed velocity, $\mu_{\ln V_s}$ is the natural log of the predicted velocity from [Equation \(12\)](#), and δb_s^* is conditional on measurements (e.g. as shown in [Fig. 11](#)).

The covariance simulation method [e.g. Refs. [36,40]] was utilised to generate spatially correlated random fields for the illustrative examples presented here. This method has a simple computational implementation compared with other common simulation methods [e.g. sequential, spectral, turning bands or circulant embedding simulation methods [40]] but comes at the expense of computational effort. The covariance simulation method has four core steps: first an n by n covariance matrix (Σ) is constructed (utilising the semivariograms developed in [Section 4](#)), second a Cholesky decomposition is used to obtain the lower triangular matrix (L) of the covariance matrix (where $\Sigma = LL^\top$), third a vector (\mathbf{u}) of length n of independent standard normal

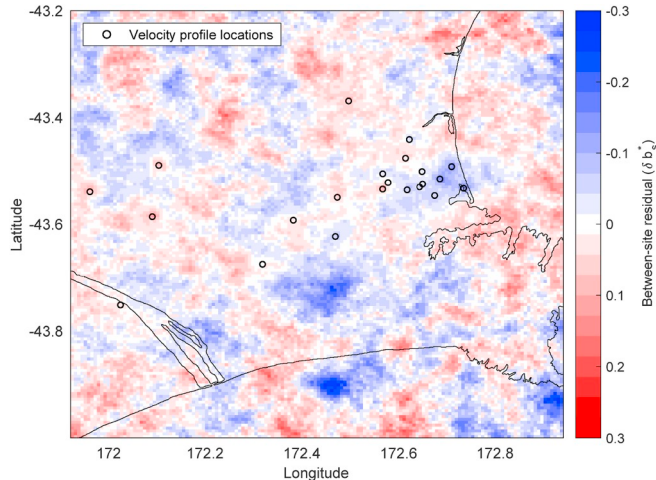


Fig. 13. Correlated δb_s^* realisation in the latitude-longitude plane.

random variables (with zero mean and unit variance) is generated, finally the random field realisation (\mathbf{V}) is calculated as $\mathbf{V} = \mathbf{L}\mathbf{u}$.

Realisations of δb_s^* and δw are simulated independently using the covariance simulation method. The entries in the covariance matrix are given by

$$\Sigma_{i,j} = \rho_{i,j} \sigma_i \sigma_j \quad (14)$$

where σ_i and σ_j are the standard deviations of the variable being simulated, at points i and j , and $\rho_{i,j}$ is the correlation (from Equation (11)). In the vertical plane when simulating δw , σ is constant and is the square-root of the variogram sill. However, in the horizontal plane, for simulating δb_s^* , σ varies by proximity to observations (see Section 4.2).

Fig. 13 presents one realisation of δb_s^* in the latitude-longitude plane in Canterbury incorporating the mean estimate of δb_s (Fig. 11) with a random field simulation component. At the locations of observed velocity profiles, the random field component is zero and δb_s^* equals the median estimate for δb_s .

Fig. 14 presents two realisations of δw in the vertical plane. Fig. 14a illustrates the near surface ($z < 100m$) structure, while Fig. 14b includes deeper maximum depths. In Fig. 14a horizontal ‘banding’ can be seen as a result of anisotropy. Fig. 14b illustrates the deep ($Z = 2km$) structure over a larger horizontal distance, and at this length scale the horizontal ‘banding’ is less apparent. However, in the vertical direction the effect of the ratio formulation for lag distance (Equation (10)) can be seen as the correlation length, the distance over which perturbations are correlated, increases with depth.

Fig. 15 presents a three-dimensional velocity model for Canterbury

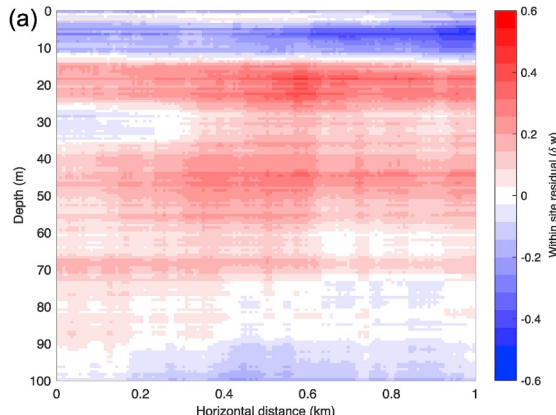


Fig. 14. Random field simulations of δw showing: (a) the near surface region ($z \leq 100m$) and (b) deep ($z \leq 2000m$) perturbations. (Note the z-axis has been exaggerated by factors of 10 and 12.5 in (a) and (b), respectively).

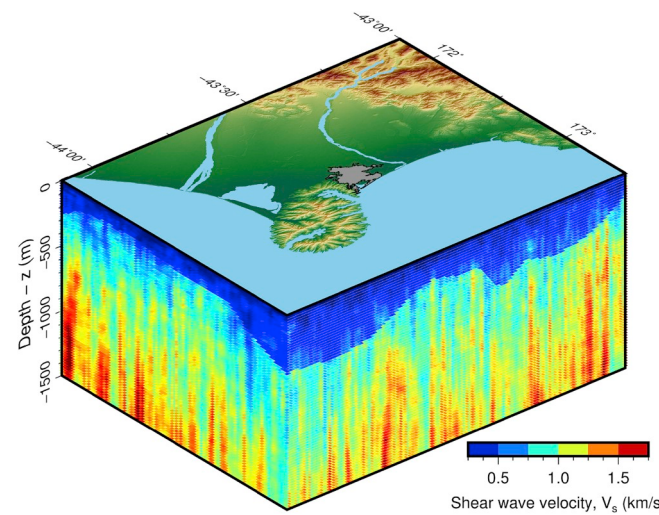


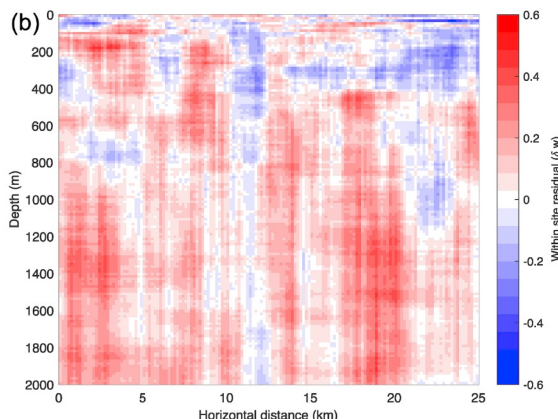
Fig. 15. Cross section of a 3D velocity model of the Canterbury with correlated velocity perturbations. Bathymetry is omitted for simplicity. (Note the z-axis has been exaggerated by a factor of 50).

[from 12] with correlated velocity perturbations (combining a randomized δb_s and a randomized δw). The large velocity contrast evident between 200m and 500m is the Gravel-Tertiary interface: above this interface gravel velocities are prescribed (Equation (9)), while below this interface the Tertiary model (Equation (7)) is used. Consideration of bathymetry was omitted in plotting. Multiple realisations of correlated velocity perturbations can be simulated to incorporate velocity uncertainty within ground motion and site response simulations [37].

5.2.1. Examination of perturbed profile dispersion curves

Fig. 16 presents the median parametric velocity profile at the site BSP and 1000 perturbed velocity profiles. Velocity perturbations were generated by simulating correlated δw realisations in the vertical direction. As perturbations are correlated with depth for a single realisation, profiles do not rapidly oscillate about the median profile. Velocities exhibit only small variations over small depths ranges (10m), while velocities can vary significantly over large depth ranges (500m).

When attempting to account for velocity uncertainty, either epistemic or aleatory/spatial, the varied velocity profiles should be consistent with the dispersion curves of the reference velocity profile in order to match the experimental site signature and for use in meaningful site response simulations [41–43]. Therefore, a comparison of the observed dispersion curves with the dispersion curves from parametric perturbed velocity profiles allows for the validity of the



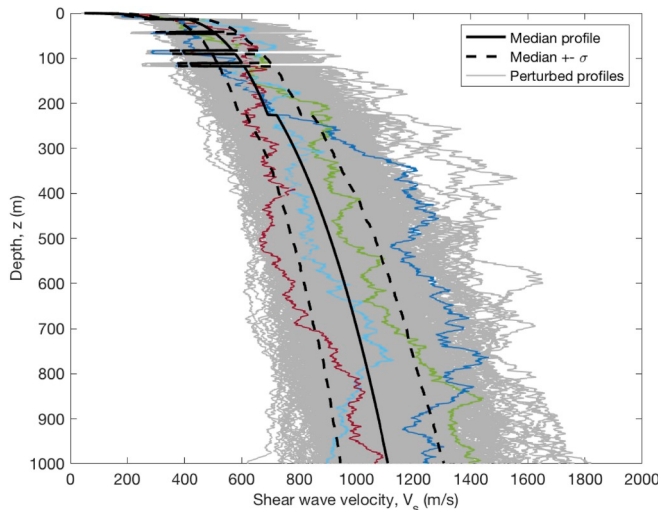


Fig. 16. Parametric velocity profile for the site BSP and 1000 realisations of correlated perturbations (four of these realisations are coloured to distinguish them from the 1000). The standard deviation was calculated directly from the 1000 velocity realisations.

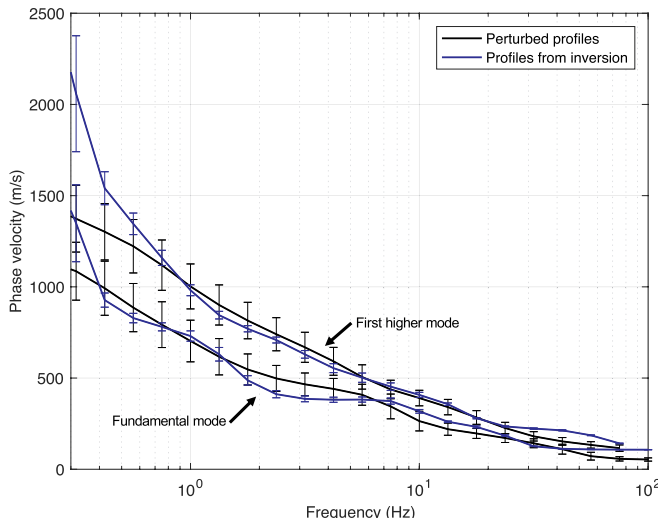


Fig. 17. Comparison of fundamental and first higher Rayleigh wave dispersion curves at site BSP for 1000 parametric perturbed profiles with 1000 velocity profiles from inversion (error bars indicate one standard deviation).

parametric velocity functions and perturbations to be investigated.

Fig. 17 presents a comparison of Rayleigh wave dispersion curves for the 1000 parametric perturbed profiles for site BSP (shown in Fig. 16) with the 1000 lowest misfit profiles from inversion [15]. For a wide frequency range (0.5 – 50 Hz) dispersion curves for the fundamental and first higher modes agree however, a deviation occurs at low frequencies (<0.5 Hz) which can be attributed to the high velocity geologic basement being present within the inversion profiles but not in the parametric perturbed profiles. The close agreement of the dispersion curves indicates the parametric perturbed velocity profiles replicate the dispersion characteristics of the lowest misfit inverted profiles and, by proxy, the experimental site signature, which informs realistic wave propagation

estimates beneath the site. As velocity perturbations (and spatial correlations) were developed without utilising dispersion data directly, the agreement of the dispersion characteristics gives confidence in the methodology utilised here to develop spatial correlations and generate velocity perturbations. Fig. 17 therefore provides qualitative evidence that the adopted approach does not suffer from the same problems noted in prior studies that have examined V_s randomisation [41–43].

The degree of agreement in the dispersion curves between (surface-wave based) data and perturbed profiles for all the considered sites was generally found to be a function of the extent to which the modelled 1D profile is consistent with velocity values used in the model development (as presented in Appendix C). Fig. 22 in Appendix C illustrates that there is a generally reasonable comparison for the BSP site, and hence the favourable comparison of perturbed dispersion curves in Fig. 17. Similarly good comparisons were also observed for approximately 40% of the considered sites (specifically 9 out of 22), with a higher proportion of inland Canterbury sites having a greater discrepancy due to differences in the velocity profiling with depth. Further research is required to assess this V_s randomisation procedure for use in downstream applications.

6. Discussion and conclusions

Parametric velocity equations for sedimentary soils in Canterbury, New Zealand, were developed using data from 22 deep shear-wave velocity profiles. The equations are able to prescribe velocities to Fine Grained Sediment, Gravels and Tertiary layer groupings. The parametric velocity equations, when combined with a regional V_{s30} model [35] and geologic surface models [11,12], enable velocity models for the Canterbury region to be generated in up to three dimensions. The equations developed prescribe shear-wave velocity, using correlations (e.g. Brocher [14]) it is possible to obtain primary-wave velocity and density.

Geostatistical techniques were utilised to develop spatial correlations which were applied to simulate random realisations of δb_s and δw , which were incorporated with parametric velocity functions to yield velocity perturbations. The dispersion characteristics of parametric perturbed velocity profiles were compared with observations and a good agreement was found over a wide frequency range. This is indicative that the velocity perturbations replicate both the velocity variability and the dispersion characteristics at a site.

The covariance simulation method was utilised to generate random fields. However although the method has a trivial implementation, it is computationally inefficient (and prohibitive for simulating large fields) compared to other methods. This is a limitation alleviated by using an alternative method (e.g. turning bands, sequential simulation) with a smaller computational burden, enabling very large 3D perturbed velocity models to be generated.

The parametric velocity equations are planned for integration into the New Zealand Velocity Model [44] to characterise velocities within the Canterbury region for use in ground motion and site response simulations. The parametric prescriptions are a significant improvement over the previous 1D and constant velocities prescriptions utilised to characterise velocities in the Interbedded and Tertiary geologic layers, respectively.

Data and resources

Detailed inversion summaries and tabulated V_s profiles for the Teague et al. [15] sites are available on the DesignSafe Website (<https://doi.org/10.17603/DS21D4D>). All other data sources are as listed in the references cited.

Acknowledgements

Financial support of this research from the University of Canterbury, QuakeCoRE, National Hazards Research Platform (NHRP), and the Royal Society of New Zealand's (RSNZ) Marsden Fund and Rutherford

Discovery Fellowship are greatly appreciated. Special thanks to the Earthquake Commission (EQC) Biennial Grant Number 14/663 and the Capability Building Fund. This project was (partially) supported by QuakeCoRE, a New Zealand Tertiary Education Commission-funded Centre. This is QuakeCoRE publication number 0474.

Appendix A. Variogram analysis

Variogram analysis is a two-step procedure in which an empirical variogram is calculated from the observed data, then a theoretical variogram is fitted to this data. Theoretical variograms can then be utilised to calculate spatial correlations and in the horizontal direction aid in Kriging a surface to represent regional velocity trends throughout Canterbury discussed further in Section 4.2.1.

Empirical variograms are calculated by comparing the variance between data separated by a given distance. As the observed data is irregularly distributed, data within specific intervals is binned and averaged to create a smooth empirical semivariogram. The distance between intervals is referred to as the lag distance (h) while the interval is the lag tolerance. Equation (A.1) presents the mathematical formulation for the empirical variogram. Where \mathbf{u} is a vector of spatial coordinates, $z(\mathbf{u})$ is the variable under consideration (in this case the velocity residuals) and \mathbf{h} is the vector of lag distances. Empirical variograms were generated by optimising the bin widths and lag distances such that each bin had a sufficient number of observations to ensure a representative mean. Theoretical variograms were fitted using a maximum likelihood technique, with the sill equalling the variance of the dataset (as for sufficiently large lag distances observations are uncorrelated therefore the sill equals the product of the standard deviations of the two variates).

$$\gamma(\mathbf{h}) = \frac{1}{2N(\mathbf{h})} \sum_{i=1}^{N(\mathbf{h})} [z(\mathbf{u}_i + \mathbf{h}) - z(\mathbf{u}_i)]^2 \quad (\text{A.1})$$

Equation (A.2) presents the functional form of the exponential variogram model adopted for the theoretical variograms, where γ is the semi-variance, h is the lag distance, c is the sill, and a is the range. The sill and range of a variogram characterise the maximum variance and length over which correlations exist, respectively. The exponential variogram model was adopted as it was found to provide the best fit amongst conventional theoretical variogram models. A zero nugget (the semivariance at zero lag distance) was also adopted as discontinuities in velocities are not expected in the horizontal or vertical directions within a given geologic layer at the spatial scale considered in this study.

$$\gamma(h) = c \left(1 - \exp\left(\frac{-h}{a}\right) \right) \quad (\text{A.2})$$

Appendix B. Vertical correlations

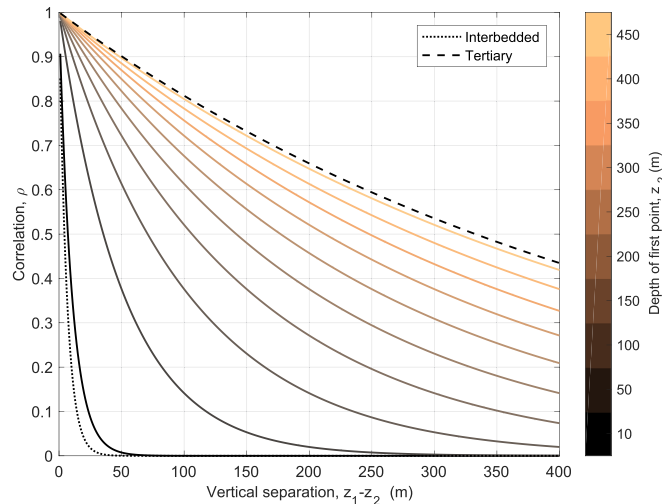


Fig. 1. Comparison of correlations for δv using the arithmetic and ratio definitions for lag distance. Correlations for the arithmetic lag formulation (dashed black lines) are shown for example variograms fitted to the Interbedded and Tertiary layer groupings; correlations using the ratio lag formulation are shown for a range of vertical separation distances. It can be seen that the correlations using the ratio lag formulation replicate those of the arithmetic lag definition.

Appendix C. Mean parametric profiles

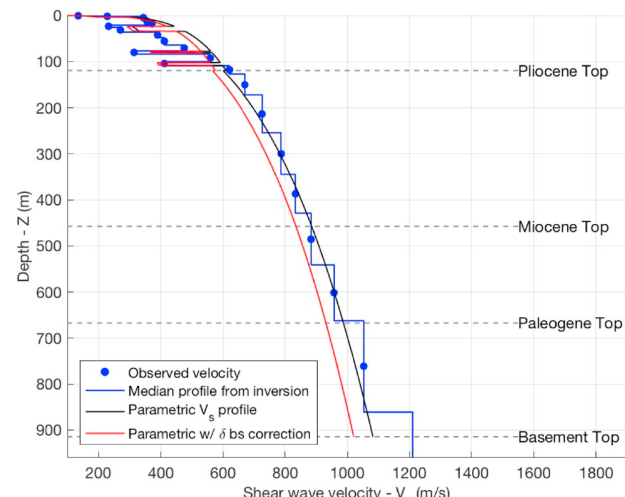
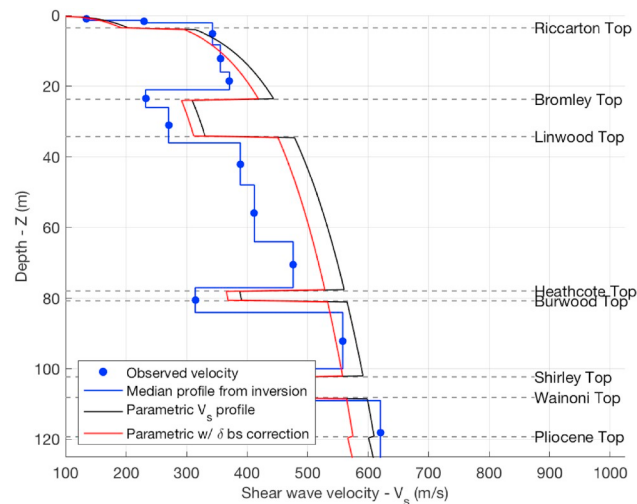


Fig. 1. Velocity profile at LINC

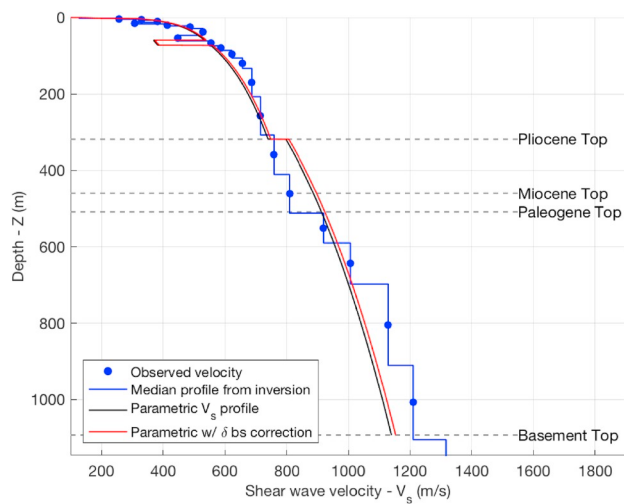
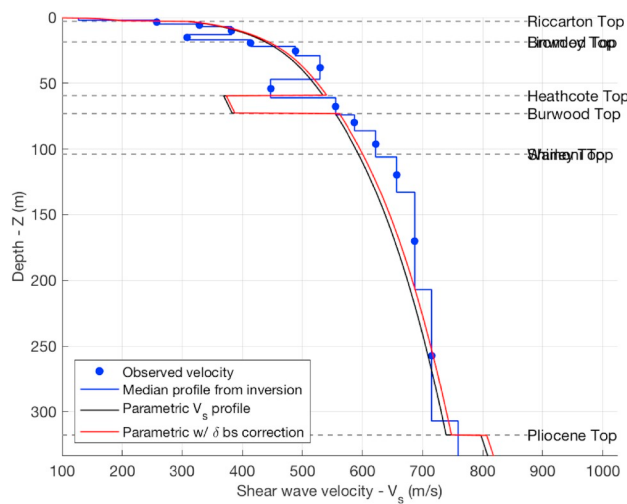


Fig. 2. Velocity profile at SLRC

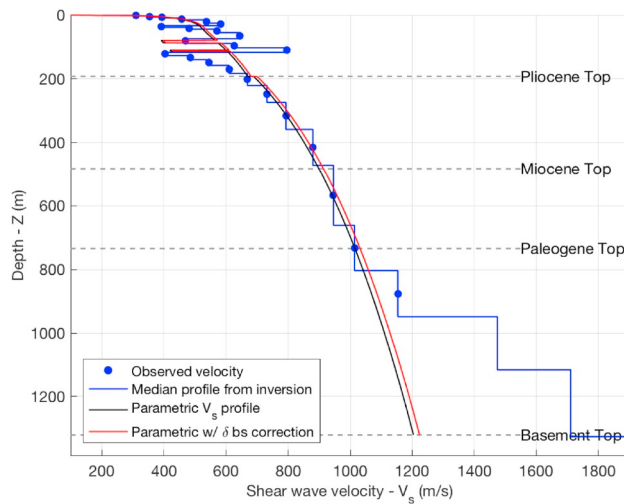
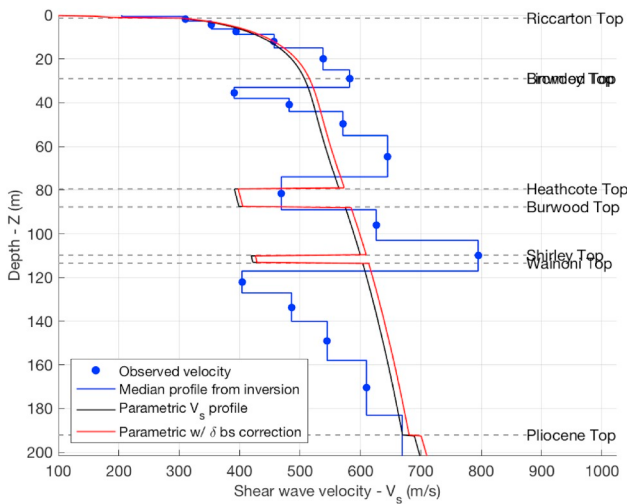


Fig. 3. Velocity profile at ROLC

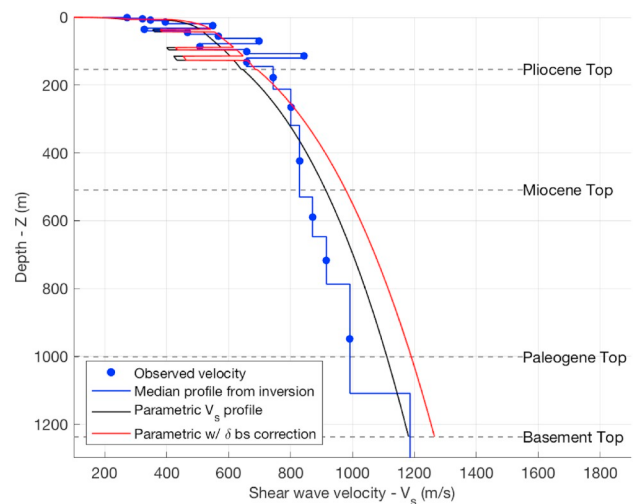
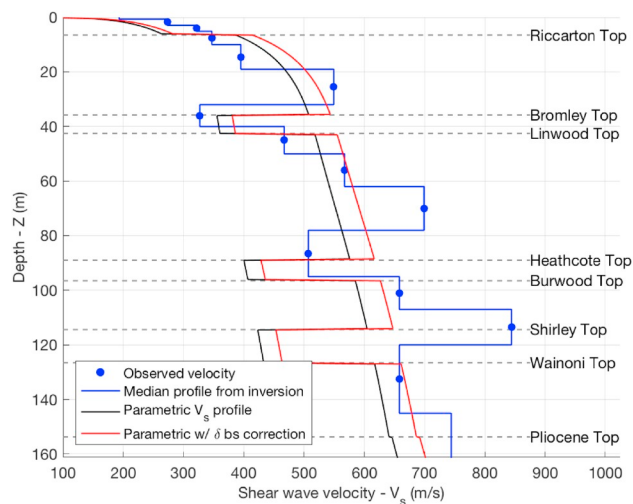


Fig. 4. Velocity profile at TPLC

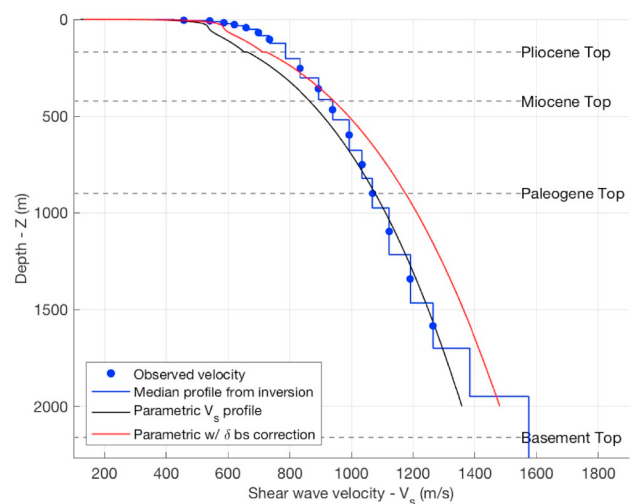
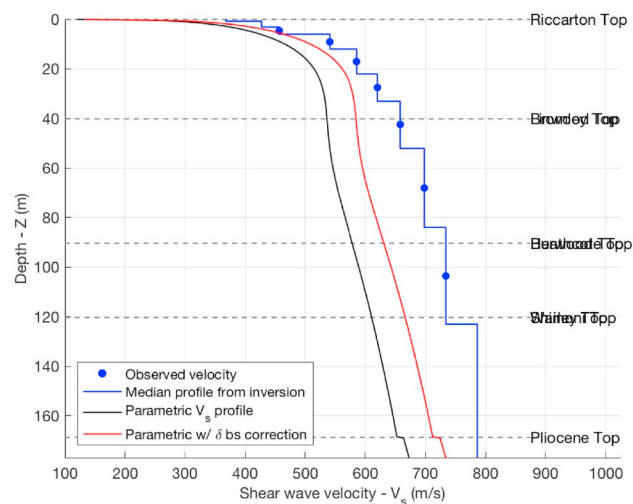


Fig. 5. Velocity profile at SWNC

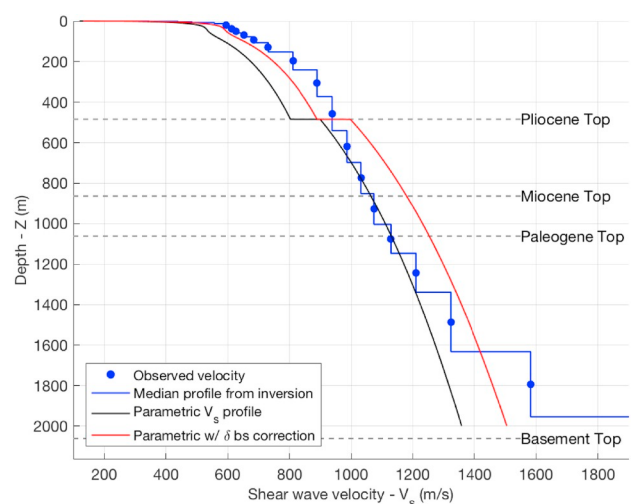
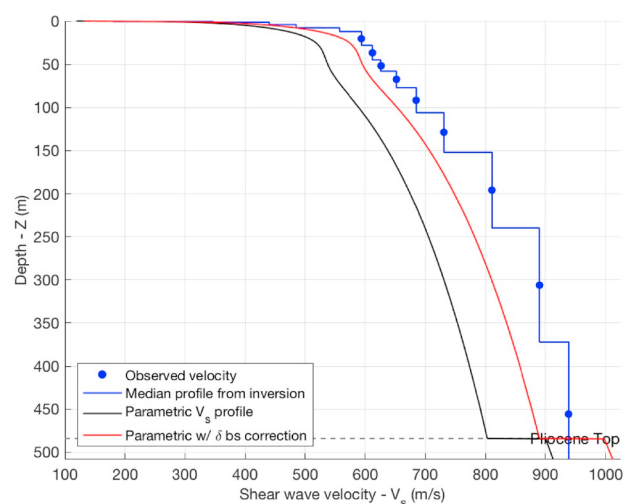


Fig. 6. Velocity profile at HORC

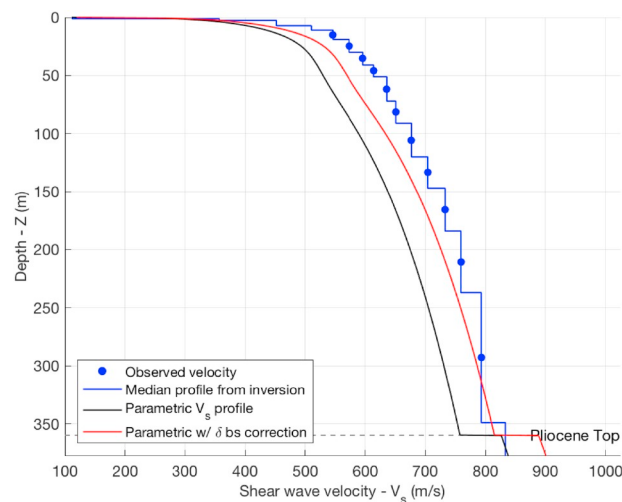


Fig. 7. Velocity profile at RKAC

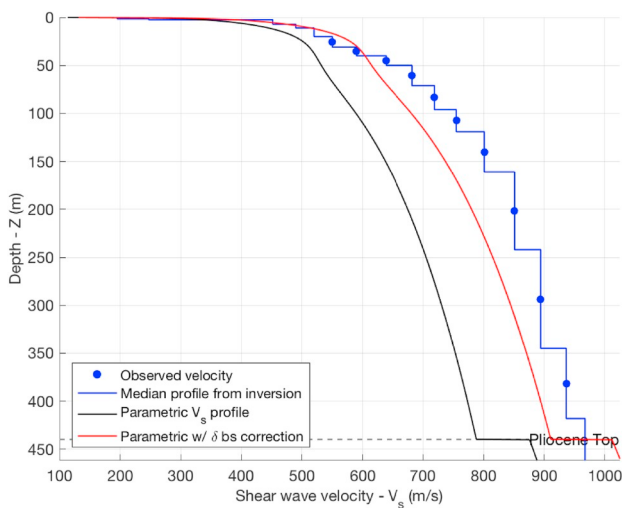
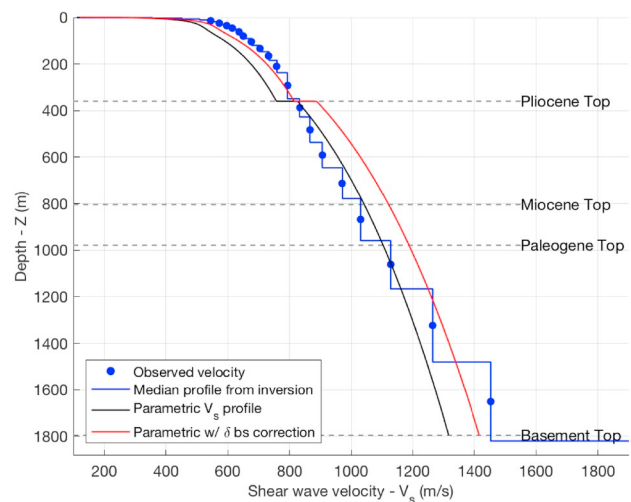


Fig. 8. Velocity profile at GDLC

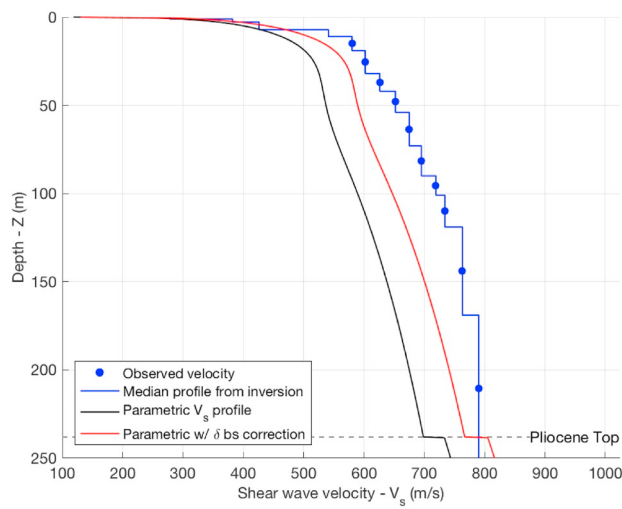
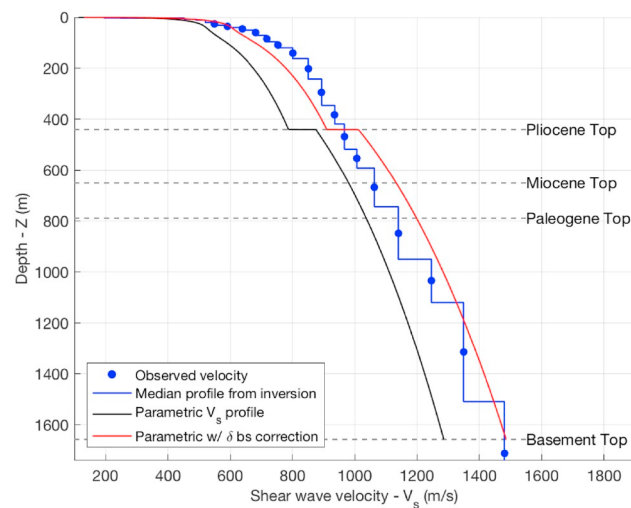


Fig. 9. Velocity profile at DFHS

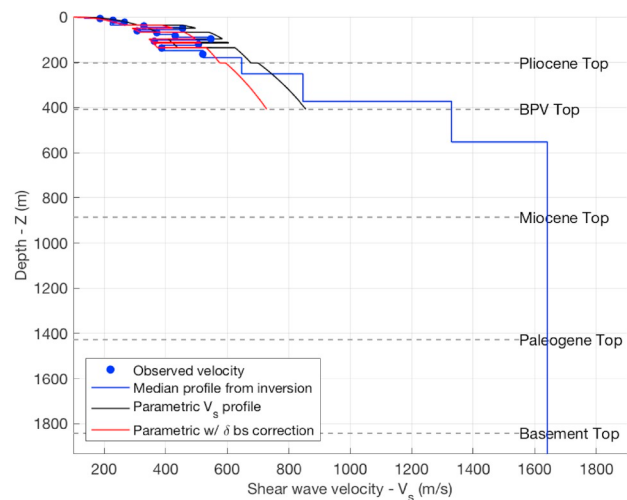
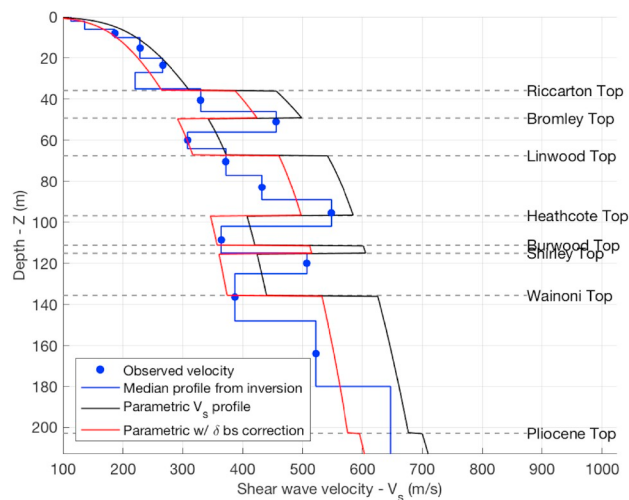


Fig. 10. Velocity profile at SNBP

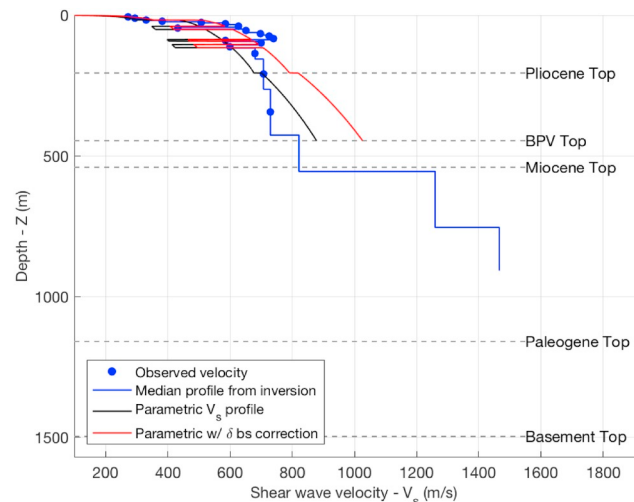
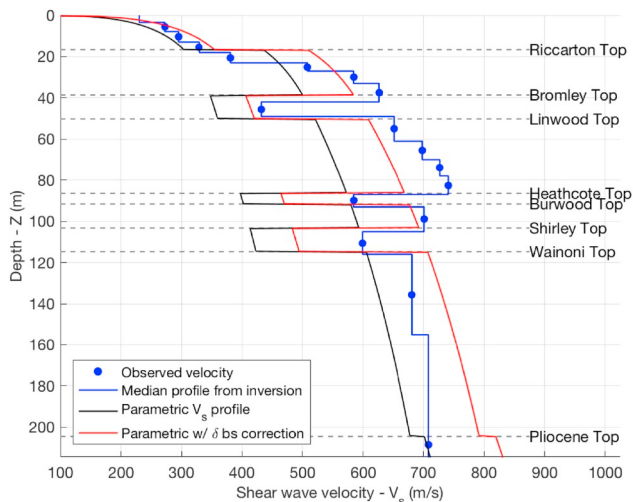


Fig. 11. Velocity profile at RHS

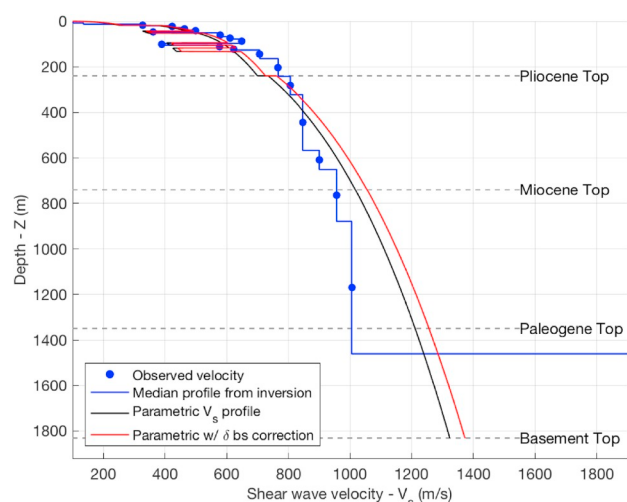
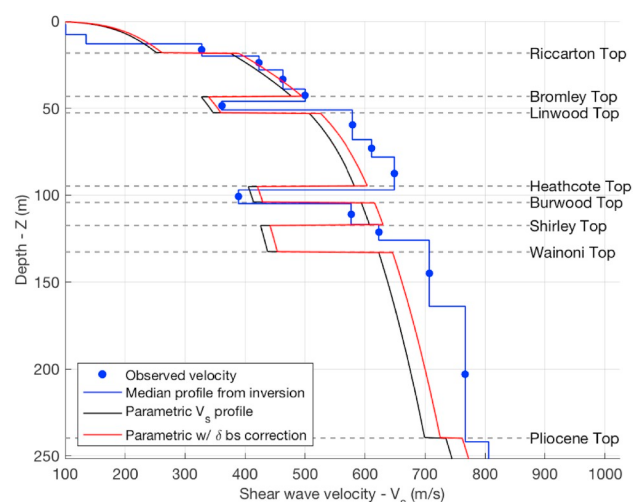


Fig. 12. Velocity profile at RWP

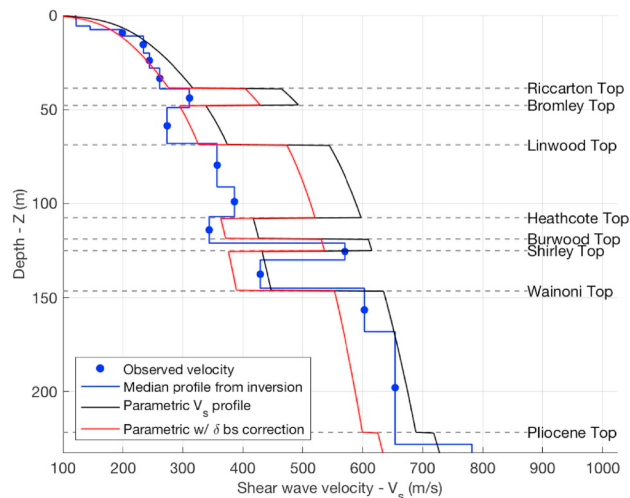


Fig. 13. Velocity profile at QEII

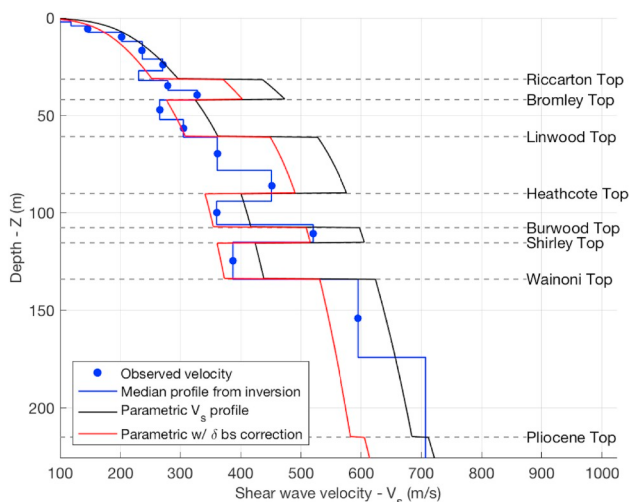
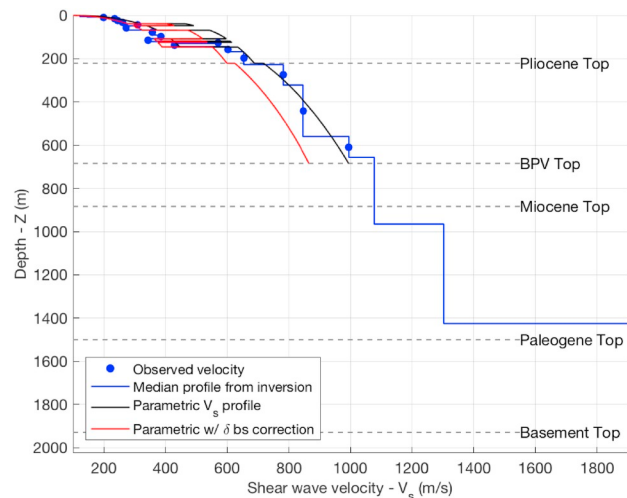


Fig. 14. Velocity profile at PP

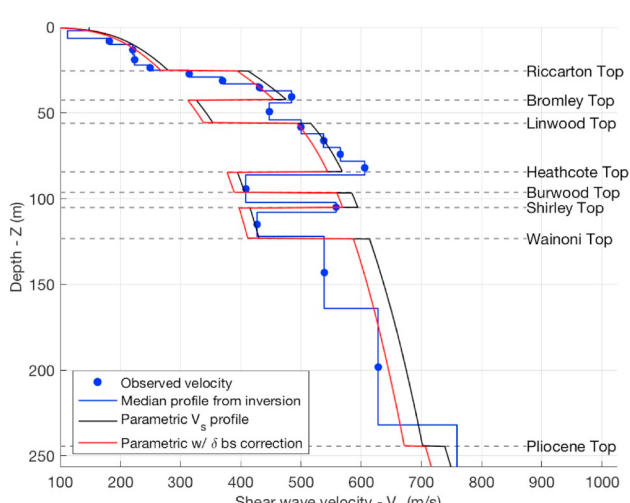
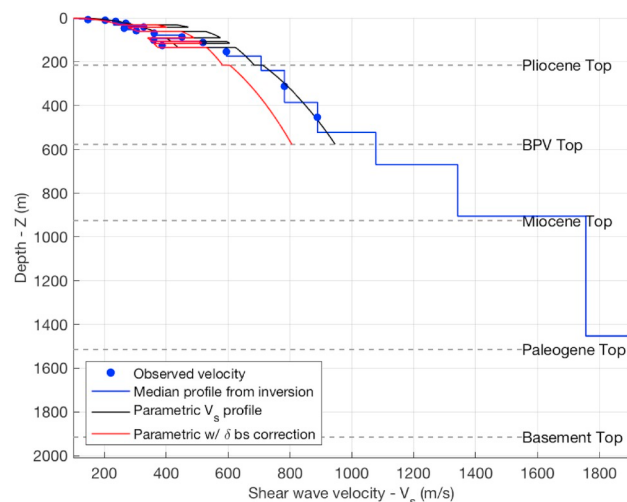
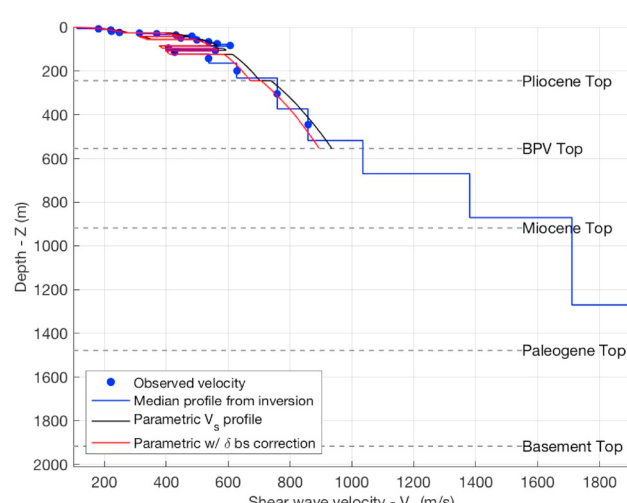


Fig. 15. Velocity profile at LS



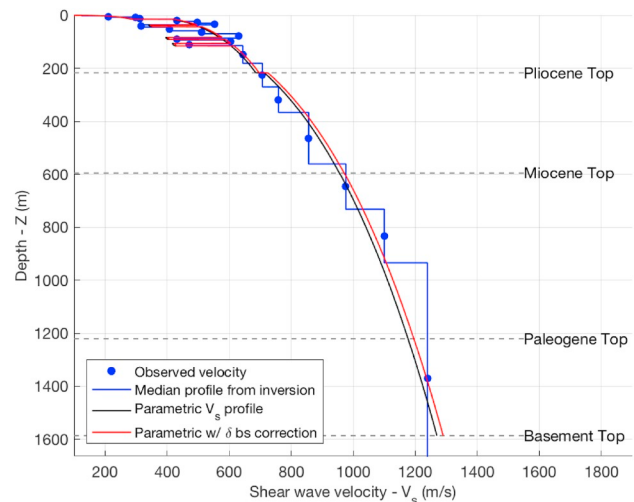
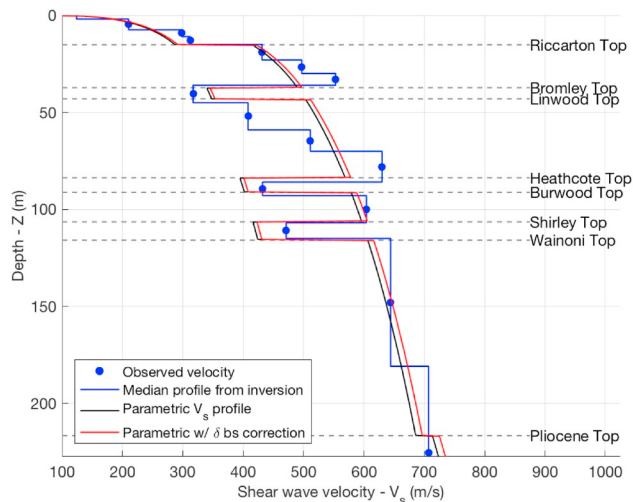


Fig. 16. Velocity profile at IF

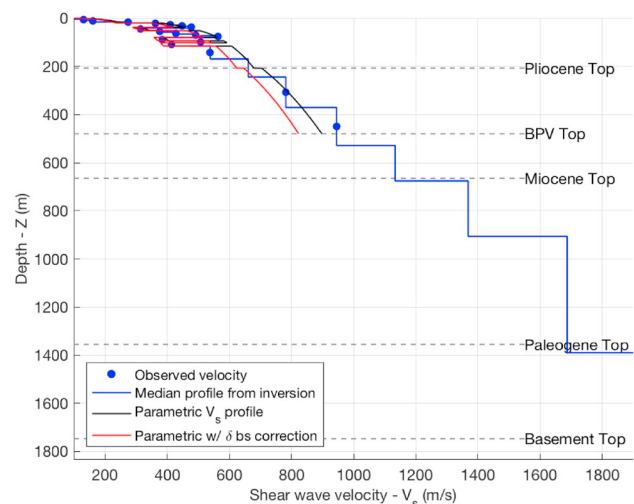
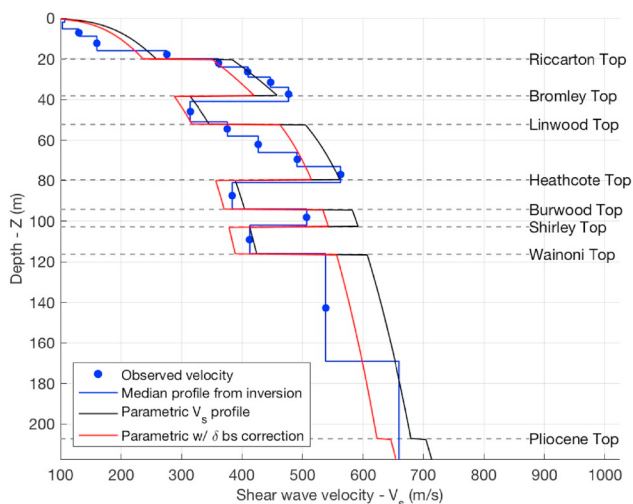


Fig. 17. Velocity profile at HP

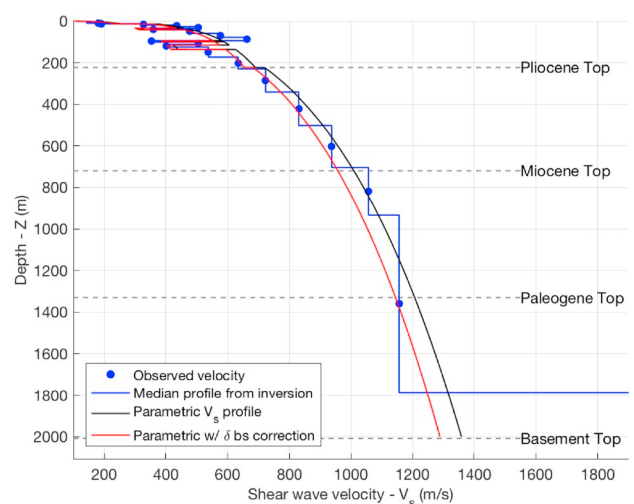
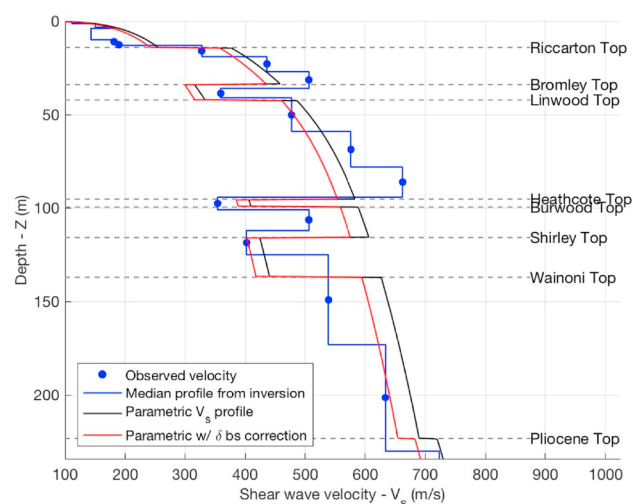


Fig. 18. Velocity profile at GRY

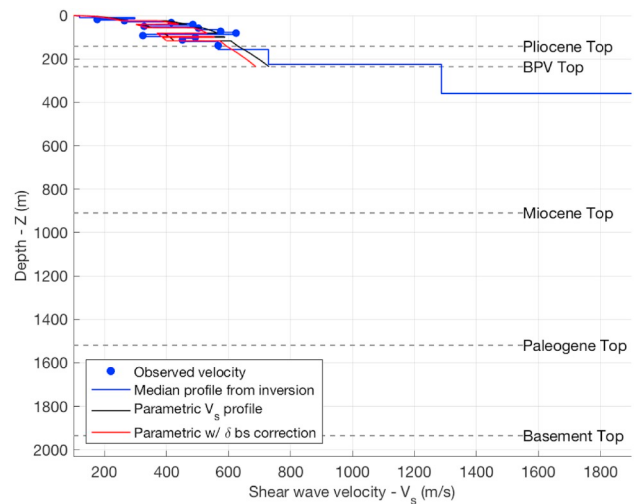
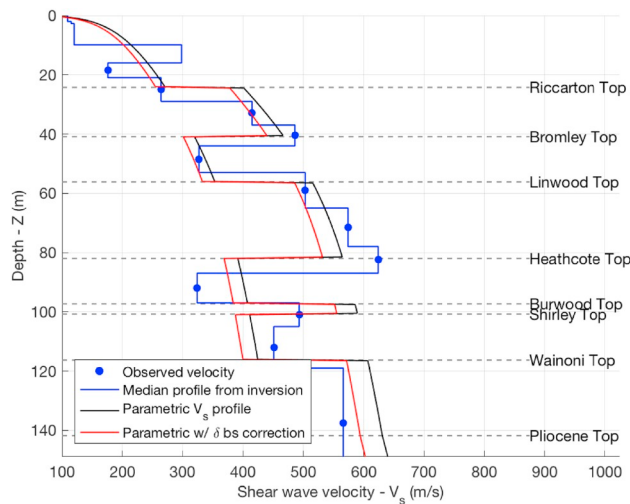


Fig. 19. Velocity profile at GP

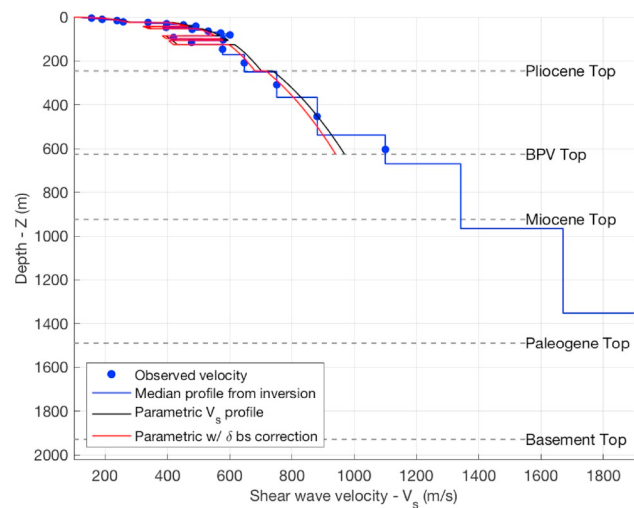
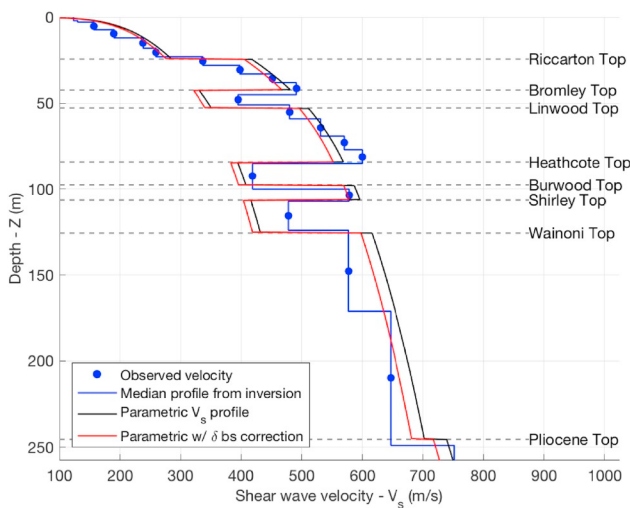


Fig. 20. Velocity profile at FTG

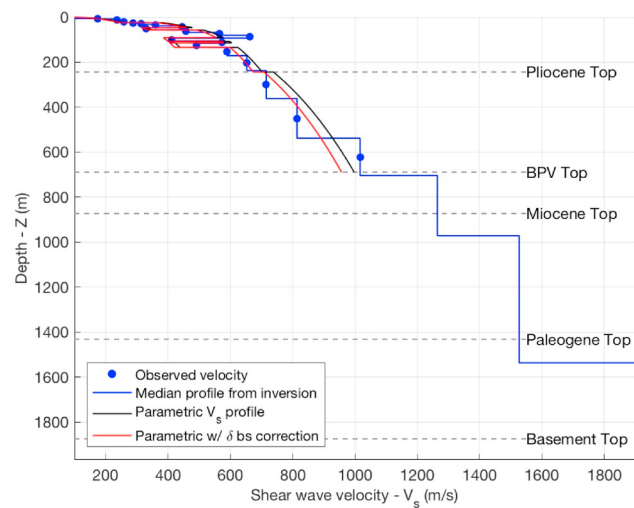
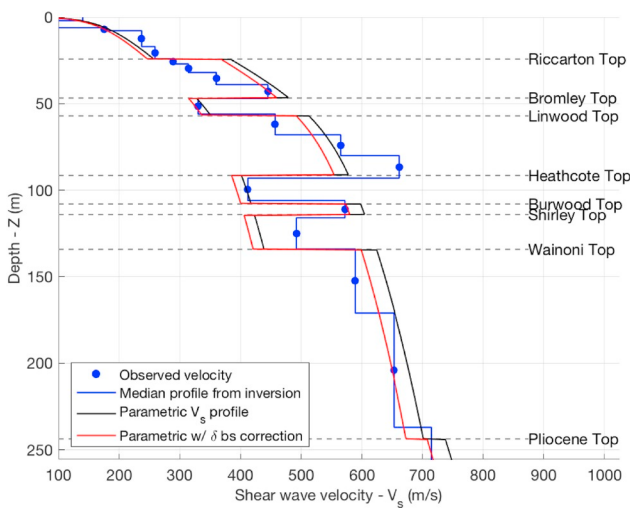


Fig. 21. Velocity profile at CCP

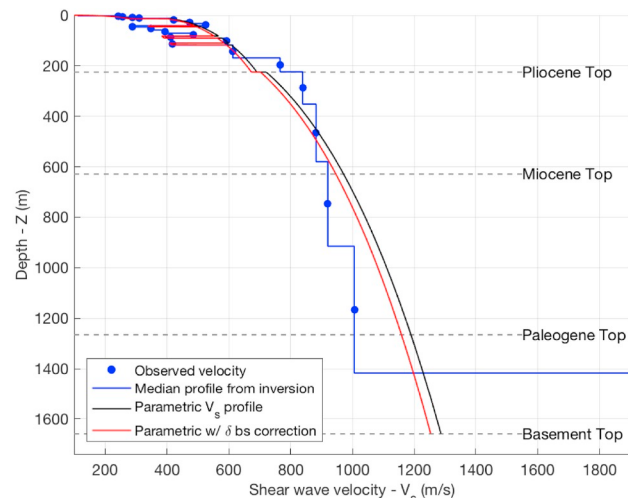
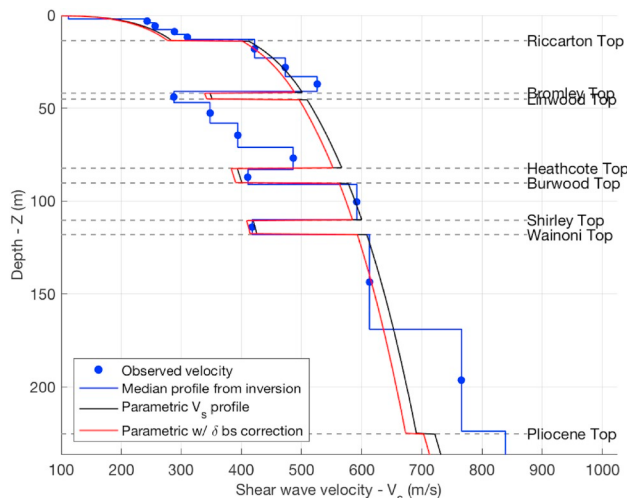


Fig. 22. Velocity profile at BSP

References

- [1] Kaiser A, Holden C, Beavan J, Beetham D, Benites R, Celentano A, Collett D, Cousins J, Cubrinovski M, Dellow G, Denys P, Fielding E, Fry B, Gerstenberger M, Langridge R, Massey C, Motagh M, Pondard N, McVerry G, Ristau J, Stirling M, Thomas J, Uma SR, Zhao J. The Mw6.2 Christchurch earthquake of February 2011: preliminary report. *N Z J Geol Geophys* 2012;55:67–90. <https://doi.org/10.1080/00288306.2011.641182>
- [2] Bradley BA, Quigley MC, Van Dissen RJ, Litchfield NJ. Ground motion and seismic source aspects of the Canterbury earthquake sequence. *Earthq Spectra* 2014;30:1–15. <https://doi.org/10.1193/030113eqs060m>. <GotoISI>://WOS:000335609300002.
- [3] Bradley BA, Cubrinovski M. Near-source strong ground motions observed in the 22 February 2011 Christchurch earthquake. *Seismol Res Lett* 2011;82:853–65. <https://doi.org/10.1785/gssrl.82.6.853>. <GotoISI>://WOS:000296544400011.
- [4] Bradley BA. Ground motions observed in the Darfield and Christchurch earthquakes and the importance of local site response effects. *N Z J Geol Geophys* 2012;55:279–86. <https://doi.org/10.1080/00288306.2012.674049>. <GotoISI>://WOS:000308250600014.
- [5] Razafindrakoto HN, Bradley BA, Graves RW. Broadband ground-motion simulation of the 2011 Mw 6.2 Christchurch, New Zealand, earthquake. *Bulletin of the Seismological Society of America*; 2018.
- [6] Bradley B, Jeong S, Razafindrakoto H. Strong ground motions from the 2010–2011 Canterbury earthquakes and the predictive capability of empirical and physics-based simulation models. 10th Pacific conference on earthquake engineering. 2015. p. 6–8.
- [7] Barnes PM. High-frequency sequences deposited during quaternary sea-level cycles on a deforming continental-shelf, north Canterbury, New Zealand. *Sediment Geol* 1995;97:131–56. [https://doi.org/10.1016/0037-0738\(94\)00141-G](https://doi.org/10.1016/0037-0738(94)00141-G). <GotoISI>://WOS:A1995RK97800002.
- [8] Barnes LJ, Weeber JH. Geology of the Christchurch urban area: Institute of Geological and Nuclear Sciences Geological Map 1. 1992. p. 1. Lower Hutt, New Zealand, Scale 25,000:1.
- [9] Forsyth P, Barrell D, Jongens R. Geology of the Christchurch area. *Institut Geol Nucl Sci* 2008;1:250. 000 geological map. 16.
- [10] Hicks S. Structure of the Canterbury plains, New Zealand, from gravity modelling. *Geophys Div, Dep Sci Indus Res* 1989. Research report no. 222.
- [11] Lee RL, Bradley BA, McGann CR. 3D models of Quaternary-aged sedimentary successions within the Canterbury, New Zealand region. *N Z J Geol Geophys* 2017;1–21.
- [12] Lee RL, Bradley BA, Ghisetti FC, Thomson EM. Development of a 3D velocity model of the Canterbury, New Zealand, region for broadband ground-motion simulation. *Development of a 3D velocity model of the Canterbury, New Zealand, region*. Bull Seismol Soc Am 2017;107:2131–50.
- [13] Barnes PM, Ghisetti FC, Gorman AR. New insights into the tectonic inversion of North Canterbury and the regional structural context of the 2010–2011 Canterbury earthquake sequence, New Zealand. *Geochem Geophys Geosyst* 2016;17:324–45.
- [14] Brocher TA. Empirical relations between elastic wavespeeds and density in the earth's crust. *Bull Seismol Soc Am* 2005;95:2081–92. <https://doi.org/10.1785/0120050077>. URL: <GotoISI>://WOS:000234412100005.
- [15] Teague D, Cox B, Bradley B, Wotherspoon L. Development of deep shear wave velocity profiles with estimates of uncertainty in the complex inter-bedded geology of Christchurch, New Zealand. *Earthquake Spectra*; 2017.
- [16] Deschenes MR, Wood CM, Wotherspoon LM, Bradley BA, Thomson EM. Development of deep shear wave velocity profiles in the Canterbury plains. New Zealand. *Earthquake Spectra*; 2018.
- [17] Aki K. Analysis of the seismic coda of local earthquakes as scattered waves. *J Geophys Res* 1969;74:615–31.
- [18] Sato H, Fehler MC, Maeda T. Seismic wave propagation and scattering in the heterogeneous earth vol. 496. Springer; 2012.
- [19] Imperatori W, Mai PM. Broad-band near-field ground motion simulations in 3-dimensional scattering media. *Geophys J Int* 2012;192:725–44.
- [20] Imperatori W, Mai PM. The role of topography and lateral velocity heterogeneities on near-source scattering and ground-motion variability. *Geophys J Int* 2015;202:2163–81. <https://doi.org/10.1093/gji/ggv281>
- [21] Graves R, Pitarka A. Kinematic ground-motion simulations on rough faults including effects of 3D stochastic velocity perturbations. *Bull Seismol Soc Am* 2016;106:2136–53.
- [22] Wotherspoon L, Orense R, Bradley B, Cox B, Wood C, Green R. Geotechnical characterization of Christchurch strong motion stations. Earthquake commission biennial grant report, project No. 12/629, Christchurch, New Zealand. 2014.
- [23] Park CB, Miller RD, Xia JH. Multichannel analysis of surface waves. *Geophysics* 1999;64:800–8. <https://doi.org/10.1190/1.1444590>. <GotoISI>://WOS:000080703600018.
- [24] Roberts JC, Asten MW. Resolving a velocity inversion at the geotechnical scale using the microtremor (passive seismic) survey method. *Explor Geophys* 2004;35:14–8. <https://doi.org/10.1071/Eg04014>. <GotoISI>://WOS:000208398300003.
- [25] Talbot J, Weeber J, Freeman M, Mason C, Wilson D. The Christchurch artesian aquifers, north Canterbury catchment board and regional water board 49. 1986.
- [26] White P, Della Pasqua F. Riccarton formation, Burnham formation and Windwhistle formation lithologies west and northwest of Christchurch city. *GNS Sci Rep* 2008;169.
- [27] Ghisetti F, Sibson R. Compressional reactivation of E–W inherited normal faults in the area of the 2010–2011 Canterbury earthquake sequence. *N Z J Geol Geophys* 2012;55:177–84.
- [28] Rodgers A, Petersson NA, Nilsson S, Sjogreen B, McCandless K. Broadband waveform modeling of moderate earthquakes in the San Francisco Bay Area and preliminary assessment of the USGS 3D seismic velocity model. *Bull Seismol Soc Am* 2008;98:969–88. <https://doi.org/10.1785/0120060407>. <GotoISI>://WOS:000254528000036.
- [29] Ramirez-Guzman L, Boyd OS, Hartzell S, Williams RA. Seismic velocity model of the central United States (version 1): description and simulation of the 18 April 2008 Mt. Carmel, Illinois, earthquake. *Bull Seismol Soc Am* 2012;102:2622–45.
- [30] Magistrale H, McLaughlin K, Day S. A geology-based 3D velocity model of the Los Angeles basin sediments. *Bull Seismol Soc Am* 1996;86:1161–6. <GotoISI>://WOS:A1996VD74600021.
- [31] Faust LY. Seismic velocity as a function of depth and geologic time. *Geophysics* 1951;16:192–206.
- [32] Lin Y-C, Joh S-H, Stoeke K. Analyst J: analysis of the UTexas 1 surface wave dataset using the SASW methodology. *Geo-congress 2014: geo-characterization and modeling for sustainability*. 2010. p. 830–9.
- [33] Bates D, Mächler M, Bolker B, Walker S. Fitting linear mixed-effects models using lme4. *J Stat Softw* 2015;67:1–48. <https://doi.org/10.18637/jss.v067.i01>.
- [34] Deschenes MR. Theses and Dissertations: Development of deep site specific and reference shear wave velocity profiles in the Canterbury plains, New Zealand vol. 2466. 2017. <https://scholarworks.uark.edu/etd/2466>.
- [35] Foster KM, Bradley BA, McGann CR, Wotherspoon LM. A Vs30 map for New Zealand based on geologic and terrain proxy variables and field measurements. *Earthquake Spectra*; 2019. In press <https://doi.org/10.1193/121118EQS281M>.
- [36] Goovaerts P. *Geostatistics for natural resources evaluation*. Oxford University Press on Demand; 1997.
- [37] Hartzell S, Harmsen S, Frankel A. Effects of 3D random correlated velocity perturbations on predicted ground motions. *Bull Seismol Soc Am* 2010;100:1415–26.

- [38] Frankel A, Clayton RW. Finite difference simulations of seismic scattering: implications for the propagation of short-period seismic waves in the crust and models of crustal heterogeneity. *J Geophys Res: Solid Earth* 1986;91:6465–89.
- [39] Thompson EM, Baise LG, Kayen RE, Guzina BB. Impediments to predicting site response: seismic property estimation and modeling simplifications. *Bull Seismol Soc Am* 2009;99:2927–49.
- [40] Remy N, Boucher A, Wu J. Applied geostatistics with SGeMS: a user's guide. Cambridge University Press; 2009.
- [41] Griffiths SC, Cox BR, Rathje EM, Teague DP. Surface-wave dispersion approach for evaluating statistical models that account for shear-wave velocity uncertainty. *J Geotech Geoenviron Eng* 2016;142:04016061[https://doi.org/10.1061/\(ASCE\)GT.1943-5606.0001552](https://doi.org/10.1061/(ASCE)GT.1943-5606.0001552)<https://ascelibrary.org/doi/abs/10.1061/%28ASCE%29GT.1943-5606.0001552>.
- [42] Griffiths SC, Cox BR, Rathje EM, Teague DP. Mapping dispersion misfit and uncertainty in vs profiles to variability in site response estimates. *J Geotech Geoenviron Eng* 2016;142:04016062[https://doi.org/10.1061/\(ASCE\)GT.1943-5606.0001553](https://doi.org/10.1061/(ASCE)GT.1943-5606.0001553)<https://ascelibrary.org/doi/abs/10.1061/%28ASCE%29GT.1943-5606.0001553>.
- [43] Teague DP, Cox BR, Rathje EM. Measured vs. predicted site response at the garner valley downhole array considering shear wave velocity uncertainty from borehole and surface wave methods. *Soil Dyn Earthq Eng* 2018;113:339–55. <https://doi.org/10.1016/j.soildyn.2018.05.031><http://www.sciencedirect.com/science/article/pii/S0267726117306772>.
- [44] Thomson EM, Bradley BA, Lee RL. Methodology and computational implementation of a New Zealand Velocity Model (NZVM2.0) for broadband ground motion simulation. *N Z J Geol Geophys* 2019;1–18<https://doi.org/10.1080/00288306.2019.1636830>.